On the theory of the strange and unconventional isotopic effects in ozone formation

Yi Qin Gao and R. A. Marcus[a)]
Noyes Laboratory, 127-72, California Institute of Technology, Pasadena, California 91125

(Received 16 April 2001; accepted 10 September 2001)

The strange mass-independent isotope effect for the enrichment of ozone and the contrastingly unconventional strong mass-dependent effect of individual reaction rate constants are studied using statistical (RRKM)-based theory with a hindered-rotor transition state. Individual rate constant ratios of recombination reactions and enrichments are calculated. The theory assumes (1) an "η-effect," which can be interpreted as a small deviation from the statistical density of states for symmetric isotopomers, compared with the asymmetric isotopomers, and (2) weak collisions for deactivation of the vibrationally excited ozone molecules. A partitioning effect controls the recombination rate constant ratios. It arises from small differences in zero-point energies of the two exit channels of dissociation of an asymmetric ozone isotopomer, which are magnified into large differences in numbers of states in the two competing exit channel transition states. In enrichment experiments, in contrast, this partitioning factor disappears exactly [Hathorn and Marcus, J. Chem. Phys. **112**, 9497 (2000)], and what remains is the η-effect. Both aspects can be regarded as "symmetry driven" isotopic effects. The two experiments, enrichments and rate constant ratios, thus reveal markedly different theoretical aspects of the phenomena. The calculated low-pressure ozone enrichments, the low-pressure recombination rate constant ratios, the effects of pressure on the enrichment, on the individual recombination rate constant ratios, and on the recombination rate constant are consistent with the experimental data. The temperature dependence of the enrichment and of the recombination rate constant ratios is discussed and a variety of experimental tests are proposed. The negative temperature dependence of the isotopic exchange rate constant for the reaction $^{16}O+^{18}O^{18}O\rightarrow{}^{16}O^{18}O+^{18}O$ at 130 K and 300 K is used for testing or providing information on the nature of a variationally determined hindered-rotor transition state. The theory is not limited to ozone formation but is intended to apply to other reactions where a symmetrical stable or unstable gas phase molecule may be formed. © *2002 American Institute of Physics.*
[DOI: 10.1063/1.1415448]

I. INTRODUCTION

Many observations have been made of isotopic effects in ozone formation from the recombination of oxygen atoms and oxygen molecules. The results are summarized elsewhere.[1] The experiments involve a "mass-independent" isotope effect in ozone formation in scrambled systems[2–24] and contrastingly different experimental results[25–29] in unscrambled systems. The latter show, instead, dramatic unconventional mass-dependent effects. Additional experiments include the effect of temperature on the low-pressure recombination rate constant, on the isotopic exchange rate constant,[30] and on the isotopic enrichments,[12] and the effect of pressure on isotopic enrichment[9,12,13,28] and on individual recombination rate constant ratios,[28] and on the rate constant.[31] The field itself may provide added insight into diverse phenomena, such as stratospheric/tropospheric mixing, oxidative processes in the stratosphere and mesosphere, interpretation of ancient and of planetary atmosphere, and other aspects.[32–35]

Both unscrambled and scrambled experiments are studied in theory. The former contain only XX and YY isotopomers of O_2, while in scrambled systems XY also exists (X,Y=^{16}O,^{17}O,^{18}O). Accordingly, in unscrambled experiments vibrationally excited ozone isotopomers XYY* are formed only from X+YY→XYY*, while in scrambled experiments they are also formed from Y+XY→XYY*. The relative importance of the two dissociation channels of XYY* in the theory[1,36,37] is determined by a "partitioning factor," which in turn depends on whether the access to XYY* is from one or both channels. This difference in conditions leads in the kinetic scheme to a marked difference in the theoretical expressions[36,37] for the two types of experiments. In the current theory[1] weak collisions play an important role. Their use in the literature for treating activation–deactivation processes[38–43] and treating pressure effects is well known.[44–49]

RRKM theory[50,51] was used as the zeroth-order theory with a small correction for the effective density of states of symmetric isotopomeric ozone molecules, XXX and XYX, as compared with the asymmetric ones YXX or YXZ. This correction is apart from the usual symmetry numbers, which are also included. The "non-RRKM" correction η is assumed to be small, the density of states for the symmetric ozone isotopomers being reduced by a factor η, chosen later

a)Electronic mail: ram@caltech.edu

to be 1.18 at 300 K, but η is large in its consequence for the ''mass-independent'' phenomenon.[1,36] More generally, an asymmetric ozone such as YXX may also show deviation from the statistical behavior, but the deviation is assumed greater for the symmetric ozones by a factor η.[1] In the symmetric XXX* or XYX* certain anharmonic vibrational coupling and Coriolis rotational–vibrational coupling terms are absent, because of symmetry restrictions, so leading to a larger nonstatistical effect for the symmetric isotopomers.[36] The coupling terms are responsible for intramolecular statistical behavior. In principle, the ''η-effect'' could also originate from collisional rather than intramolecular properties.[1] We amplify on this point later.

In a weak collision model rate equations are obtained for the population density of the vibrationally excited ozone molecules as a function of the energy E and of the total angular momentum J. We use a strong collision model for the collisional angular momentum transfer of ozone, and obtain a one-dimensional energy space model for ozone. A similar reduction has been used for unimolecular dissociation.[52]

An important quantity in weak collisions is the average energy $\langle \Delta E \rangle$ of downward transfer ΔE for deactivating collisions. Energy transfer is typically described by this $\langle \Delta E \rangle$ and is relatively insensitive to the possible functional form of the energy transfer.[44,45] For simplicity, we use a step-ladder model, in which energy is transferred between the excited ozone molecule and a bath gas molecule in discrete steps of ΔE per collision. At low pressures only one collision is important during the lifetime of a vibrationally excited ozone molecule and so then only energetic ozone molecules with energy less than ΔE above the threshold lead to a deactivated ozone.

We also consider the isotopic exchange reaction of ozone: Information about the transition state for any recombination reaction, such as $^{16}O+^{32}O_2 \rightarrow ^{48}O_3$, would normally be obtained from the magnitude and temperature dependence of its high pressure rate constant. However, the behavior of the ozone formation rate constant k_{bi} versus third-body pressure is complex at high pressures,[31] and cannot be used for this purpose. Instead, we can obtain information from low pressure data on the isotopic exchange reactions,[30,53,54]

$$^{16}O+^{18}O_2 \rightarrow ^{16}O^{18}O+^{18}O. \tag{1.1}$$

The negative temperature coefficient[30] of its rate constant shows that the transition state is not ''loose,'' meaning that the rotation of the reacting diatomic molecule in the transition state is hindered: A free rotation leads to a positive or only an extremely small negative temperature dependence.[37]

The theory is also used to treat three pressure effects on ozone formation: the effect on individual recombination rate constant ratios for forming ozone isotopomers,[28] on the isotopic enrichment,[9,12,13,28] and on the rate of the recombination reaction $^{16}O+^{32}O_2 \rightarrow ^{48}O_3$ at different temperatures.[31] The temperature effect on the isotopic enrichment[12] and on the individual recombination rate constant ratios is also discussed.

In summary, in the present paper we build on two previous papers from our group[36,37] and adds new features: (1) a weak collision model, using a step-ladder model for deactivating and activating collisions, (2) a hindered-rotor variational transition state, which is also compared with the results from a free rotor, and (3) the treatment of a greater variety of experimental effects as a consequence, such as pressure and temperature effects. Earlier the room temperature data on ratios of reaction rates were treated with very encouraging results,[37] but because of the limitations of a loose transition state and of a strong collision model, an *ad hoc* assumption was introduced: The calculated rate constant ratios at room temperature were assumed to equal those at 130 K, where the transition state is indeed nearly loose.[37] This assumption is eliminated in the present paper.

We use extensively equations[36] relating the enrichments to the ratios of recombination rate constants. This relation is independent of approximations such as hindered versus free rotor and weak versus strong collisions. A chemical kinetic scheme was used to obtain it[36] and is essential in any treatment of observables such as enrichments. The need for a scheme has sometimes been overlooked in the literature.

The paper is organized as follows: the kinetic scheme, a master equation approach, and the treatment of the hindered-rotor transition state theory are described in Sec. II. Expressions are obtained for the individual recombination reaction rate constants, the enrichments δ and E,[36] and the rate constants of isotopic exchange reactions. A numerical and partially analytic procedure is used for treating pressure effects for a recombination reaction. The expressions are used in Sec. III to calculate rate constants, enrichments, and pressure and temperature effects, and the results are discussed in Sec. IV, which also contains a simple explanation of how small differences in zero-point energies of the competing exit channels of the dissociating molecule are magnified into large unusual mass-dependent isotopic effects. Temperature effects on isotopic enrichments and on rate constant ratios are also discussed there. Several experiments are suggested to test different aspects of the theory.

II. THEORY

A. Kinetic scheme and rate constants

For the ozone formation we have the kinetic scheme

$$X+YZ \rightarrow XYZ(EJ), \quad k_r^a(EJ), \tag{2.1}$$

$$XYZ(EJ)+M \rightarrow XYZ(E'J')+M, \quad \omega(EJ \rightarrow E'J'), \tag{2.2}$$

$$XYZ(E'J') \rightarrow X+YZ, \quad k_d^a(E'J'), \tag{2.3}$$

$$XYZ(E'J') \rightarrow XY+Z, \quad k_d^b(E'J'), \tag{2.4}$$

and, in a series of steps to form a stable ozone molecule of energy E^l,

$$XYZ(EJ)+M \rightarrow XYZ(E^l,J')+M, \quad \omega(EJ \rightarrow E^l,J'), \tag{2.5}$$

where E^l is any energy sufficiently below the dissociation threshold that the XYZ has a negligible chance of reacquiring enough energy to dissociate. Only E and total angular momentum J are conserved in individual reaction steps (2.1), (2.3), and (2.4). The $k_r^a(EJ)$, $k_d^a(EJ)$, and $k_d^b(EJ)$ are E- and

J-dependent rate constants of the recombination and dissociation reactions, respectively, and $\omega(EJ\rightarrow E'J')$ is the rate per unit E of forming XYZ at $(E'J')$ from (EJ) by a collision with a third body M. The units of $k_r^a(EJ)$ are $(\text{energy})^{-1}$ $(\text{concentration})^{-1}$ $(\text{time})^{-1}$, and those of k_d^a are $(\text{time})^{-1}$.

For the dissociation of XYZ* there exist the two distinguishable exit channels a and b when X≠Z. For a symmetric molecule, where X=Z, the designation (a,b) is omitted. By convention,[36,37] channel a is the one with the lower zero-point energy of the diatomic species. Thus, the YZ in Eq. (2.3) has a lower zero-point energy than the XY in (2.4).

We let $c(EJ)$ denote the concentration of ozone molecules in quantum states having any specified (EJ) per unit energy E. The rate equation for a distribution function $g(EJ)$, defined as $c(EJ)/[\text{X}][\text{YZ}]$, is[55]

$$\frac{dg(EJ)}{dt}=k_r^a(EJ)-[k_d^a(EJ)+k_d^b(EJ)+\omega]g(EJ)+\sum_{J'}\int_{E'}\omega(E'J'\rightarrow EJ)g(E'J')dE', \quad (2.6)$$

where $g(EJ)$ has units of $(\text{energy concentration})^{-1}$ and ω denotes the total collision frequency,

$$\omega=\sum_{J'}\int\omega(EJ\rightarrow E'J')dE'. \quad (2.7)$$

The step-ladder model for $\omega(EJ\rightarrow E'J')$ is introduced later.

B. Expressions for $k_r(EJ)$ and $k_d(EJ)$

We consider first a general formulation which includes triatomic molecules as a special case. A molecule with total energy in $(E,E+dE)$ and total angular momentum J is formed from the reacting pair. The energy $E_n^J(q)$ of a particular quantum state nJ along the reaction coordinate q has a maximum at some $q^\dagger$, and its energy there is denoted by E_n^J. In a recombination step, the probability of finding a pair of reactants with the specified J and in a phase space volume element $dq\,dp$ for motion along q is $(2J+1)\times\exp(-E/k_BT)dq\,dp/hQ_a$, where Q_a is the partition function for the colliding pair. To obtain the incident probability flux we divide by dq and multiply by $\dot{q}$, the velocity along the reaction coordinate. The contribution to the rate constant from this J and energy range $(E,E+dE)$ is obtained by summing over all accessible states n of the transition state. The recombination rate constant $k_r(EJ)$ is then

$$k_r(EJ)=N(EJ)e^{-E/k_BT}/hQ, \quad (2.8)$$

where

$$N(EJ)=(2J+1)\sum_n h(E-E_n^J), \quad (2.9)$$

and $h(E-E_n^J)$ is a unit step function. We used the relation $\dot{q}\,dp=(p/\mu)dp=d(p^2/2\mu)=dE$, μ being the reduced mass of motion along q, and then divided by dE to obtain a rate per unit E. Equations (2.8) and (2.9) are equivalent to an earlier result for bimolecular collisions.[56] When the reaction path leads to two different molecules and so bifurcate, Eq. (2.9) requires a modification given later.

Particularly in large systems it has been convenient to choose the position of the transition state to be at a $q^\dagger$ which depends only on J and E.[57] In this case Eq. (2.8) again applies but $N(EJ)$ now denotes all accessible states at the given q. The q now is chosen to minimize $N(EJ)$ (variational RRKM theory). Sometimes it is convenient to choose the position of the transition state so as to be determined by EJ and by some quantum numbers whose totality is denoted by α. In that case Eqs. (2.8)–(2.9) become, instead,

$$k_r(EJ)=\sum_\alpha N(EJ\alpha)e^{-E/k_BT}/hQ_a, \quad (2.10)$$

where $N(EJ\alpha)$ is the number of quantum states of a specified transition state $EJ\alpha$ and the $q^\dagger$ for each $(EJ\alpha)$ is determined variationally.

We consider next the rate constant for the dissociation of a vibrationally excited molecule. For any quantum state n the number of quantum states along q is again $dq\,dp/h$, and dividing by dq and multiplying by $\dot{q}$ we again have $\dot{q}\,dp/h$, i.e., dE/h. The number of quantum states of the parent molecule at the given $(E,E+dE)$ and J is $\rho(EJ)dE$, where $\rho(EJ)$ is the density of the quantum states of the dissociating molecule, and each quantum state (nJ) of the transition state thereby contributes a value $h(E-E_n^J)/h\rho(EJ)$ to the dissociation rate constant $k_d(EJ)$,[57,58] and so we have

$$k_d(EJ)=N(EJ)/h\rho(EJ), \quad (2.11)$$

where $N(EJ)$ is again given by Eq. (2.9) and the $\rho(EJ)$ contains a $(2J+1)$ factor.

When the states are grouped together so that all states of the same $EJ\alpha$ are taken to have the same position of the transition state Eqs. (2.9) and (2.11) yield

$$k_d(EJ)=\sum_\alpha N(EJ\alpha)/h\rho(EJ). \quad (2.12)$$

When all quantum states are taken to have the same value of $q^\dagger$, Eq. (2.12) yields the usual variational RRKM expression,

$$k_d(EJ)=N(EJ)/h\rho(EJ). \quad (2.13)$$

To treat the $k_r^a(EJ)$ in Eq. (2.1) for ozone formation we consider an energetic ozone molecule XYZ formed from X+YZ with given J and in the energy range $(E,E+dE)$ in the center of mass system of coordinates. This $k_r^a(EJ)$ is given by Eqs. (2.8)–(2.9) for the homonuclear case, X+YY→XYY, with a superscript a added to the $k_r(EJ)$ and $N(EJ)$. In the heteronuclear case, X+YZ→XYZ with Z≠Y, two reaction products, XYZ* and XZY*, can form. The rate constant for forming XYZ* then contains a weighting function introduced onto the right-hand side of Eq. (2.8), as discussed in Appendix A. The quantum numbers n of the transition state consist of J, its spaced-fixed projection M_J, the principal quantum number of the hindered rotation j, the quantum number Ω of the transition state that corresponds to the body-fixed projection of J along the axis of least moment of inertia, and the vibrational quantum number of the oxygen fragment. Before collision four appropriate quantum numbers of the colliding pair were the diatomic rotation quantum number, the orbital quantum number of the colliding pair,

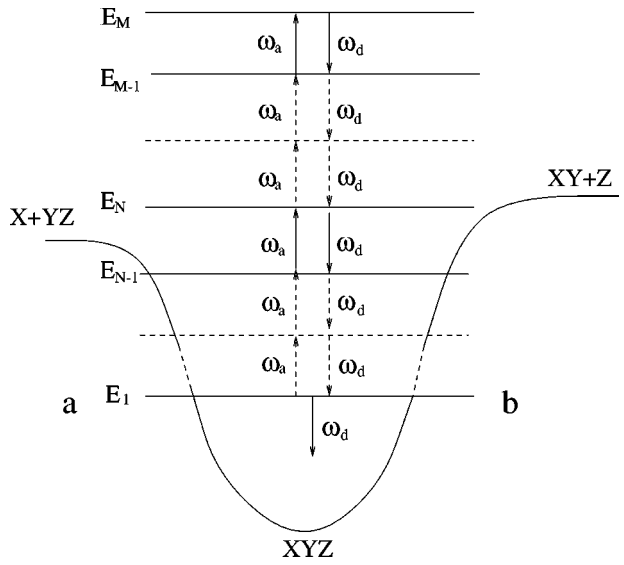

FIG. 1. The step-ladder model for the deactivation of XYZ* molecules formed by the recombination reaction. The schematic curve is the sum of the potential energy and the local zero-point energy.

and their projections on space-fixed axes. They are now replaced by $JM_J\Omega j$. The M_J gives rise to the well known $2J+1$ factor in Eq. (2.8). The sum over n is now a sum over j and Ω. The vibrational quantum number of the O_2 fragment at $q^\dagger$ can be taken as zero.

The $k_d^a(EJ)$ in Eq. (2.3) is the rate constant for dissociation of the vibrationally excited XYZ* back into the incident channel X+YZ. Modifying Eqs. (2.8) and (2.9), it is given by

$$k_d^a(EJ)=N_a(EJ)/h\rho(EJ)$$

$$=(1/2)\sum_{j\Omega}(2J+1)h(E-E_{j\Omega}^{J,a})/h\rho(EJ), \quad (2.14)$$

where $N_a(EJ)$ is the number of quantum states in the transition state of XYZ*→X⋯YZ→X+YZ which arise from this dissociation of XYZ*. The 1/2 in Eq. (2.14) occurs only when YZ is heteronuclear.[59] The sum in Eq. (2.14) over j and Ω is subject to the restrictions $|\Omega|\leqslant j$ and $|\Omega|\leqslant J$. For the $k_d^b(EJ)$ in Eq. (2.4) for the dissociation of XYZ* to XY+Z, the a in Eq. (2.14) is replaced by b, and now the sum is over the $j\Omega$ states of the exit channel b.

C. Step-ladder model for the collisional energy transfer

The step-ladder model is depicted schematically in Fig. 1: only a certain amount of energy ΔE is transferred from an ozone molecule to a bath molecule per collision, and there is a ladder of M steps for the energies $E_n=E_1+(n-1)\Delta E$, $n=1,2,\ldots,M$. The M is some upper cut-off beyond which any contribution to ozone formation is negligible. E_1 is chosen so that states with energies less than E_1 are sufficiently below the dissociation threshold that their probability of reacquiring energy to dissociate is negligible. They are treated together as a sink. The energy of this lowest step E_1 is later varied to ensure that the calculated rate constant converges to a finite value. There exist an infinite number of sets of ladders, each differing in their energy within the interval ΔE. We first obtain the solution for a single ladder which begins with any particular energy E_1. The total rate constant is obtained by integrating over E_1 in the interval ΔE.

A deactivating collision in the step-ladder model can be written as

$$\omega(E'J'\rightarrow EJ)=\omega_d t(J'\rightarrow J)\,\delta(E'-E-\Delta E), \quad (2.15)$$

where ω_d is the deactivation collision frequency, treated as a constant in the region close to the dissociation threshold, which is the region of interest. The $t(J'\rightarrow J)$ is the transition probability from J' to J and equals $P(J)$ when a strong collision is assumed for rotational angular momentum transfer. $P(J)$ is the thermal distribution of the rotational states J of XYZ at the given temperature.[52] The frequency ω_a for activation collisions is related to ω_d by microscopic reversibility, and satisfies (Appendix B)

$$\omega_d\rho(E)e^{-\Delta E/k_BT}=\omega_a\rho(E-\Delta E), \quad \rho(x)=\sum_J \rho(xJ). \quad (2.16)$$

For a range of energies near the dissociation threshold, $\rho(E)$ is approximated by a constant, and Eq. (2.16) becomes $\omega_a=\omega_d e^{-\Delta E/k_BT}$. The total collision frequency ω in Eq. (2.6) is $\omega_a+\omega_d$.

In a step-ladder and strong rotational collision model the population density $g(E_nJ)$ of XYZ at E_nJ, obtained from Eqs. (2.6) and (2.15), satisfies

$$k_r^a(E_nJ)-[k_d^a(E_nJ)+k_d^b(E_nJ)+\omega]g(E_nJ)$$
$$+P(J)\omega_d g_{n+1}+P(J)\omega_a g_{n-1}=0, \quad (2.17)$$

in the steady-state approximation[55] $dg(E_nJ)/dt=0$. Each g_n denotes

$$g_n=\sum_J g(E_nJ). \quad (2.18)$$

Upon dividing Eq. (2.17) by $k_d^a(E_nJ)+k_d^b(E_nJ)+\omega$ and summing over J we obtain a one-dimensional master equation:

$$g_n=U_n+V_ng_{n+1}+W_ng_{n-1}, \quad (2.19)$$

where

$$U_n=\sum_J \frac{k_r^a(E_nJ)}{k_d^a(E_nJ)+k_d^b(E_nJ)+\omega}, \quad (2.20)$$

$$V_n=\sum_J \frac{P(J)\omega_d}{k_d^a(E_nJ)+k_d^b(E_nJ)+\omega}, \quad (2.21)$$

$$W_n=\sum_J \frac{P(J)\omega_a}{k_d^a(E_nJ)+k_d^b(E_nJ)+\omega}. \quad (2.22)$$

The flux below the threshold is treated analytically in Appendix C (cf. Ref. 60). We next treat Eqs. (2.19)–(2.22) in the low pressure limit.

D. Recombination at low pressures

For energies E_n above the dissociation threshold D_0, there are "open" and "closed" states for dissociation, according as $k_d^a(E_nJ)+k_d^b(E_nJ)>0$ or $k_d^a(E_nJ)+k_d^b(E_nJ)=0$, respectively. The effective dissociation barrier height for a state depends on J because of the J-dependent centrifugal barrier.[61] To avoid zero denominators in the low-pressure limit in Eqs. (2.19)–(2.22), it is necessary to keep track of the two types of states.

The rate equations for the population density $g^c(E_nJ)$ of the closed states are obtained by setting $k_r^a=0$ and $k_d^a+k_d^b=0$ in Eq. (2.17), which now contains only collisional terms. Upon summing over J, Eq. (2.17) then yields

$$P_n^c\omega_d g_{n+1}-\omega g_n+P_n^c\omega_a g_{n-1}=-\omega g_n^o, \tag{2.23}$$

where P_n^c is the sum of $P(J)$ over the closed J states at E_n, and g_n and g_n^o are given by Eqs. (2.25) and (2.26),

$$P_n^c=\sum_J^c P(J), \tag{2.24}$$

$$g_n=g_n^o+g_n^c, \tag{2.25}$$

where

$$g^o=\sum_J g^o(E_nJ), \quad g_n^c=\sum_J g^c(E_nJ). \tag{2.26}$$

When $E_n<D_0$, the P_n^c in Eq. (2.23) is unity, since only closed states exist, and $g_n^o=0$. Thereby,

$$\omega_d g_{n+1}-\omega g_n+\omega_a g_{n-1}=0, \quad 1<n\leqslant N-1, \tag{2.27}$$

and for $n=1$,

$$\omega_d g_2-\omega g_1=0. \tag{2.28}$$

Since states with energy less than E_1 are treated together as a sink, their total population density grows at a rate S,

$$S=\omega_d g_1. \tag{2.29}$$

The rate constant for the formation of a stable ozone molecule equals the integral of $\omega_d g_1$ over the step size ΔE, and has the usual bimolecular reaction rate constant units of (concentration)$^{-1}$ (time)$^{-1}$. This bimolecular rate constant itself can be a pressure-dependent pseudo-rate constant.

We consider next the open states in the low-pressure limit. The collision terms in Eq. (2.17) are now small compared with the terms containing k's and can be neglected, so that for the open states we have

$$g^o(E_nJ)=\frac{k_r^a(E_nJ)}{k_d^a(E_nJ)+k_d^b(E_nJ)}. \tag{2.30}$$

Summing Eq. (2.30) over these open states yields

$$g_n^o=\sum_J \frac{k_r^a(E_nJ)}{k_d^a(E_nJ)+k_d^b(E_nJ)} \quad (N\leqslant n\leqslant M). \tag{2.31}$$

Equations (2.23) and (2.27)–(2.29) constitute a system of $(N-1)+2(M-N+1)$ linear equations for the same number of variables. $M-N+1$ of these variables are given explicitly by Eq. (2.31), leaving M closed g_n to be determined from the remaining equations. An analytic relation between N of the variables is given in Appendix C. The remaining equations yield an expression for the population density g_1 in Eq. (2.29). The low-pressure recombination rate constant for channel a is obtained by integrating $\omega_d g_1$ over the step size ΔE in Appendix C:

$$k_{bi}^{0,a}=\frac{\omega_d-\omega_a}{Q_a}\left(\int_0^{\Delta E}\sum_J \rho(EJ)Y_a(EJ)\times e^{-E/k_BT}\frac{\omega}{\omega_d+\omega_a P^o(E)}dE+\int_{\Delta E}^{2\Delta E}\sum_J \rho(EJ)Y_a(EJ)\times e^{-E/k_BT}\frac{\omega_d P^c(E-\Delta E)}{\omega_d+\omega_a P^o(E-\Delta E)}dE+\cdots\right), \tag{2.32}$$

where

$$Y_a(EJ)=N_a(EJ)/[N_a(EJ)+N_b(EJ)] \tag{2.33}$$

is the partitioning factor,[1,36,37] $P^o(E)=1-P^c(E)$, and $P^c(E)$ denotes P_N^c. The states with energies higher than $2\Delta E$ have negligible contributions to Eq. (2.32) at low pressures (cf. Appendix B) and can be neglected.

E. Effective rate constants and enrichments in scrambled systems

When YZ and XY are both present we can write for the formation of a stabilized ozone molecule of structure XYZ,

$$\frac{d\mathrm{XYZ}}{dt}=k_{bi}^{0,a}\mathrm{X}\cdot\mathrm{YZ}+k_{bi}^{0,b}\mathrm{Z}\cdot\mathrm{XY}. \tag{2.34}$$

When there is a rapid equilibrium between atomic and diatomic species this equation becomes

$$\frac{d\mathrm{XYZ}}{dt}=k_{bi}^{\mathrm{eff},a}\mathrm{X}\cdot\mathrm{YZ}, \tag{2.35}$$

where

$$k_{bi}^{\mathrm{eff},a}=k_{bi}^{0,a}+k_{bi}^{0,b}K_{ex}=k_{bi}^{0,a}+k_{bi}^{0,b}\frac{Q_b}{Q_a}, \tag{2.36}$$

and K_{ex} is the equilibrium constant for reaction $\mathrm{X}+\mathrm{YZ}\rightleftharpoons\mathrm{Z}+\mathrm{XY}$. The $k_{bi}^{\mathrm{eff},a}$ appears as $k_{6,q6}^{\mathrm{as}}+k_{q,66}^{\mathrm{as}}K_{\mathrm{ex}}$ in the isotopic enrichment δ in Refs. 36 and 37. The superscript as in the latter denotes the formation of the asymmetric isotopomer.

Equations (2.32) and (2.36) lead to

$$k_{bi}^{\mathrm{eff},a}=\frac{\omega_d-\omega_a}{Q_a}\left(\int_0^{\Delta E}\sum_J \rho(EJ)e^{-E/k_BT}\times h[N_a(EJ)+N_b(EJ)]\times\frac{\omega}{\omega_d+\omega_a P^o(E)}dE+\int_{\Delta E}^{2\Delta E}\sum_J \rho(EJ)h[N_a(EJ)+N_b(EJ)]\times e^{-E/k_BT}\frac{\omega_d P^c(E-\Delta E)}{\omega_d+\omega_a P^o(E-\Delta E)}dE\right). \tag{2.37}$$

A similar expression is obtained for $k_{bi}^{\mathrm{eff},b}$, with Q_a replaced by Q_b. The partitioning factors Y_a and Y_b defined in Eq. (2.33) are seen to have disappeared in the k_{bi}^{eff}, an exact result, just as they did in the strong collision model of Refs. 36 and 37. The various enrichments are then calculated from Eq. (2.37) using expressions for ${}^{Q}\delta$ and ${}^{M}E$ in Refs. 36 and 37.[62]

F. Pressure dependence of rate constants and enrichments

We next solve Eqs. (2.19)–(2.22) for the g_n's at any given pressure. As long as a finite ω is retained in the denominators in these equations it is no longer necessary to use the open or closed labels to avoid zero denominators.

For the *M*-ladder system described in Fig. 1, the ozone formation rate constant is again given by the $\omega_d g_1$ in Eq. (2.29), and a method for obtaining g_1 is given in Appendix D. In the high-pressure limit, U_n, V_n, and W_n in Eqs. (2.20)–(2.22) become $U_n=\Sigma_J k_r^a(E_nJ)/\omega$, $V_n=\omega_d/\omega$, and $W_n=\omega_a/\omega$, respectively, and yield the usual high-pressure recombination rate constant k_{bi}^{∞},

$$k_{bi}^{\infty}=\frac{1}{Q_a h}\sum_J \int_E N_a(EJ)e^{-E/k_{\mathrm{B}}T}dE. \tag{2.38}$$

G. The isotopic exchange reaction and the hindered-rotor transition state

The rate constant k_{ex}^a of the isotopic exchange reaction, Eq. (1.1), is[37]

$$k_{\mathrm{ex}}^a=\frac{1}{hQ_a}\sum_J \int_E \frac{N_a(EJ)N_b(EJ)}{N_a(EJ)+N_b(EJ)}e^{-E/k_{\mathrm{B}}T}dE, \tag{2.39}$$

where Q_a is the partition function of the reacting pair in the center of mass system of coordinates for channel *a*, and $N_{a(b)}(EJ)$ is the number of states of the transition state for exit channel $a(b)$ of ozone dissociation at the given *E* and *J*. Each of the two exit channels has its own transition state (TS).

III. RESULTS

A. Isotopic exchange reaction rate constant

To implement Eq. (2.39) a potential energy surface is needed, particularly for configurations appropriate to the hindered rotational transition state. The longer O–O bond length of $O_3^{\dagger}$ in this region is estimated in the calculations given below to be in the neighborhood of 2.6 Å. *Ab initio* calculations of the potential energy surface for ozone have been optimized mainly for configurations near the equilibrium configuration or near the equilateral triangle one, where a conical intersection occurs.[63] However, an extrapolated potential energy surface near the transition state gives a poorer result[64] for the temperature coefficient of the isotopic exchange rate constant, as did an empirically modified version.[64] The modification[65] eliminated the potential energy barrier in the extrapolated surface: The absence of a barrier is clear from the observed negative temperature coefficients of the recombination and isotopic exchange rate constants. Instead, we use a very simplified model potential energy surface in Appendix E to fit the isotopic exchange reaction rate constant at both room and low (130 K) temperatures, and later for all other reactions. When an improved potential energy surface becomes available, this approximation can be removed. A new potential energy surface has recently been developed and used to calculate resonances.[66] It will be interesting to see how well its use reproduces the negative temperature dependence of the isotopic exchange reaction rate constant.

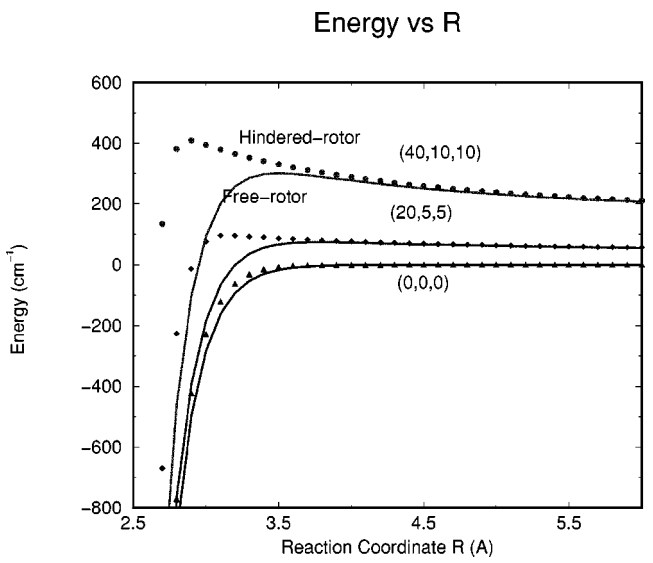

FIG. 2. The total energy $E(Jj\Omega;R)$ of a hindered rotor state $(Jj\Omega)$ as a function of *R* for ${}^{16}\mathrm{O}\cdots{}^{16}\mathrm{O}{}^{16}\mathrm{O}$. The maximum of the hindered rotor states (symbols) are shifted inward compared to that of a free rotor (JjK) (solid lines), increasingly shifted with increasing $(Jj\Omega)$.

The hindered-rotational potential in Eq. (A3) and Appendix E yield elements of the Hamiltonian matrix. The energies of the hindered rotational states are its eigenvalues $E(Jj\Omega;R)$ for the state $|Jj\Omega\rangle$,

$$E(Jj\Omega;R)=\frac{J(J+1)-2\Omega^2}{2\mu R^2}\hbar^2+\epsilon(j\Omega;R), \tag{3.1}$$

where the first term is the orbital term (cf. Appendix A) and $\epsilon(j\Omega;R)$ is an eigenvalue of a two-dimensional hindered rotor state with quantum numbers *j* and Ω. The $\epsilon(j\Omega;R)$ is obtained numerically and depends on *R*, partly via the hindered-rotor potential $V_{\mathrm{bend}}(R,\theta)$.

The hindered-rotor eigenvalues $E(Jj\Omega;R)$ plus a bond fission potential $V_{\mathrm{bf}}(R)$ are plotted versus *R* in Fig. 2, where they are compared with those of a free rotor for the same $(Jj\Omega)$. The transition state for each quantum state is seen to move to smaller *R* with increasing *E*, as expected from other studies.[67–79] The maximum of $E(Jj\Omega;R)+V_{\mathrm{bf}}(R)$ along *R* for a state with quantum numbers $(Jj\Omega)$ is denoted by $E_{j\Omega}^J$. The $N_a(EJ)$ in Eq. (2.39) is now given by

$$N_a(EJ)=\frac{1}{2}(2J+1)\sum_j \sum_{\Omega} h(E-E_{j\Omega}^J-E_0^a), \tag{3.2}$$

where the 1/2 is absent when the YZ in XYZ*→X+YZ is homonuclear (cf. Ref. 59). The effect of the hindered rota-

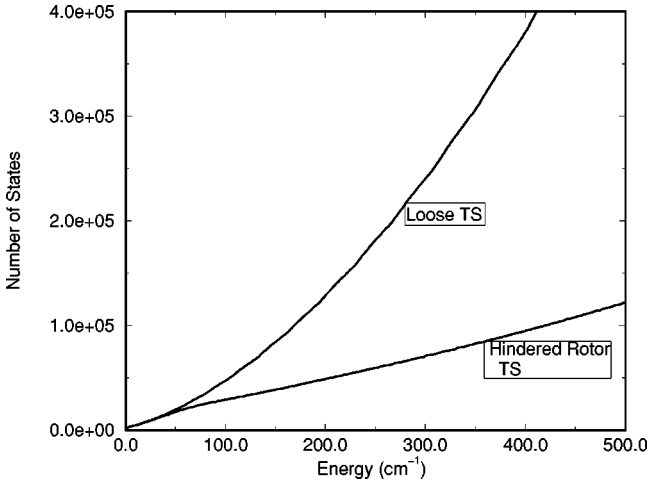

FIG. 3. The number of states N as a function of R for the recombination reaction $^{16}O+^{32}O_2 \rightarrow ^{48}O_3$. The upper curve is obtained using free rotation in the transition and the lower curve is obtained using the hindered-rotor transition state described in Appendices A and E.

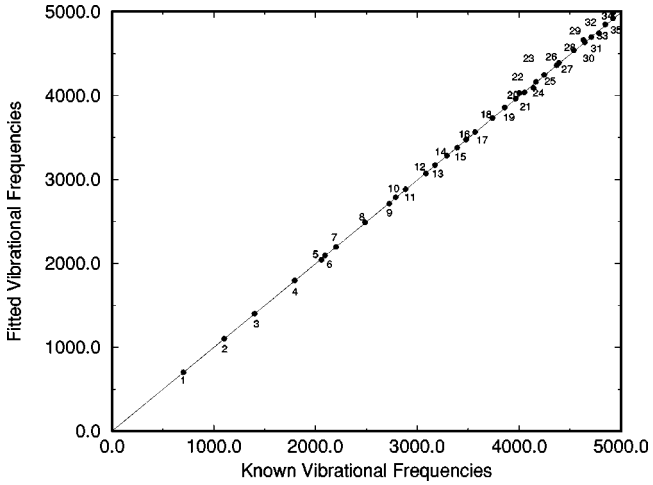

FIG. 4. The fit of the known vibrational frequencies (Ref. 85) (taken from Ref. 83) of $^{16}O^{16}O^{16}O$ using up to second-order anharmonicity corrections.

tional barrier is illustrated in Fig. 3, which gives a plot for the term $N_aN_b/(N_a+N_b)$ as a function of energy for X+YZ, Z≠Y. The plot is similar to the plot of N for a symmetric system XXX*→X···XX.

The rate constant for the isotopic exchange reaction obtained from Eq. (2.39) yields the results for 130 K and 300 K in Table I, together with the experimental results and the loose transition state results. The ΔE and η are absent in the equation used for the isotopic exchange rate constant.

B. Anharmonicities and other properties

The density of states for ozone ρ is obtained[37] from a convolution[44,45,49,80] of the rotational and vibrational density of states. The vibration frequencies of the ozone isotopomers used in the calculation were obtained using a second-order perturbation formulation, which gives the unknown frequencies to an accuracy of about 1 cm^{-1}.[81] The present calculation of density of states $\rho(EJ)$ includes anharmonicity. The latter was obtained using vibrational quantum state energies of $^{48}O_3$. The energy of a state with vibrational quanta $(v_1v_2v_3)$ is given by[82]

$$E(v_1v_2v_3)=\sum_{i=1}^{3} hc\omega_i\left(v_i+\frac{1}{2}\right)+\sum_{i=1}^{3} hcx_{ii}\left(v_i+\frac{1}{2}\right)^2+\sum_{j>i}\sum_{i=1}^{2} hcx_{ij}\left(v_i+\frac{1}{2}\right)\left(v_j+\frac{1}{2}\right), \quad (3.3)$$

and is fitted to the data in Ref. 83 up to 6000 cm^{-1}. The fit[84] to the vibrational frequencies is given in Fig. 4. The total number of states in the range of 0 to 2000 cm^{-1} above the dissociation threshold is calculated with and without inclu-

TABLE I. Calculated and experimental rate constants.

k	Reaction	T (K)	Expt.	Calc. (present)	Calc. (strong or loose)
k_{bi}^{0} [a]	$^{16}O + {}^{32}O_2 + N_2 \rightarrow {}^{48}O_3 + N_2$	130	4[b]	5.2[c]	7.0[d]
	$k_{bi} \propto T^{-n}$	130−300	$n=2.6$	$n=2.3$	$n=0.77$
		300	0.5[b]	0.76[c]	3.7[d]
k_{ex} [e]	$^{16}O + {}^{18}O^{18}O \rightarrow {}^{16}O^{18}O + {}^{18}O$	130	5.6[f]	4.3[g]	9.2[h]
		300	2.9[f]	2.7[g]	9.5[h]
	$k_{ex} \propto T^{-m}$	130−300	$m=0.88\pm0.26$	$m=0.53$	$m=-0.07$
k_{bi}^{∞} [e]	$^{16}O+{}^{32}O_2 \rightarrow {}^{48}O_3$	130	18[b]	10.4[i]	21.7[j]
		300	>4[b]	6.5[i]	20.6[j]

[a]Units are 10^{-33} cm^6 s^{-1}.
[b]Experimental data from Hippler *et al.*, Ref. 31.
[c]Calculated from Eq. (2.32) using a value of 210 cm^{-1} for ΔE. η is 1.13 at 130 K. When $\Delta E=180$ cm^{-1} the values are 4.1, 0.59 and when $\Delta E=250$ cm^{-1} the values are 5.4, 1.1. The results obtained for k_{bi}^0 and n using a free rotor transition state are, for the weak collision case, exactly the same as those given in the first three rows of the penultimate column in this Table.
[d]Calculated using the strong collision assumption.
[e]Units are 10^{-12} cm^3 molecule^{-1} s^{-1}.
[f]Experimental data from Wiegell *et al.*, Ref. 30.
[g]Calculated from Eq. (2.39) using the hindered-rotor transition state.
[h]Calculated using the loose transition state.
[i]Calculated from Eq. (2.38) using the hindered-rotor transition state.
[j]Calculated from Eq. (2.38) using the loose transition state.

TABLE II. Relative rate coefficients of an atom plus homonuclear diatomic formation channels ($X + YY \rightarrow XYY$ relative to $X + XX \rightarrow X_3$) at low pressure at 300 K.

Reaction	Expt.[a]	Cal.
$^{16}O + {}^{36}O_2 / {}^{16}O + {}^{32}O_2$	1.53 ± 0.03	1.53
$^{17}O + {}^{36}O_2 / {}^{17}O + {}^{34}O_2$	1.29 ± 0.07	1.36
$^{16}O + {}^{34}O_2 / {}^{16}O + {}^{32}O_2$	1.23 ± 0.03	1.38
$^{17}O + {}^{32}O_2 / {}^{17}O + {}^{34}O_2$	1.01 ± 0.05	1.01
$^{18}O + {}^{34}O_2 / {}^{18}O + {}^{36}O_2$	1.00 ± 0.06	1.04
$^{18}O + {}^{32}O_2 / {}^{18}O + {}^{36}O_2$	0.90 ± 0.03	0.90

[a]From Mauersberger *et al.*, Ref. 26.

sion of the anharmonicity. This 2000 cm^{-1} is more than the maximum range of energy needed for the present study of ozone formation reaction. An averaged factor of 1.5 is obtained as the anharmonic correction to the harmonic density, and was taken to be the same for all ozone isotopomers.

Also needed in the equations for the rate constants are the sums of states for the hindered-rotor, the partition function for the collision pair given by Eqs. (4.8)–(4.12) in Ref. 37, and the collision frequencies. The Lennard-Jones collision frequency is used with a unit collision efficiency and is given by Eq. (4.14) of Ref. 37.

C. Individual rate constant ratios

The individual low-pressure rate constants at 300 K for the formation of XYZ molecules are calculated for each channel using Eq. (2.32). A small η-effect was assumed for the formation of the symmetric ozones by dividing the values obtained from Eq. (2.32) by η. The values of η and of ΔE were chosen to fit two experimental low-pressure recombination rate constant ratios, $^{16}O + {}^{18}O{}^{18}O / {}^{16}O + {}^{16}O{}^{16}O$ and $^{18}O + {}^{16}O{}^{16}O / {}^{18}O + {}^{18}O{}^{18}O$. Using the hindered-rotor transition state the values $\eta = 1.18$ and $\Delta E = 210$ cm^{-1} are obtained and yield the results shown in Tables II–IV and in Figs. 5 and 6. When a free rotor transition state is used instead with $\eta = 1.18$ and $\Delta E = 260$ cm^{-1}, the results for the rate constant ratios for these free-rotor systems at these low pressures agreed to within ± 0.02 of the values for the hindered-rotor using $\Delta E = 210$ cm^{-1} in Tables II and III for all reactions.

The sensitivity of the rate constant ratio to the choice of ΔE was tested using other values, 180 cm^{-1} and 250 cm^{-1}. The calculated rate constant ratio for $^{16}O + {}^{36}O_2 \rightarrow {}^{16}O{}^{18}O{}^{18}O / {}^{16}O + {}^{32}O_2 \rightarrow {}^{16}O{}^{16}O{}^{16}O$ was 1.55, 1.53, and 1.50 when ΔE was 180, 210, and 250 cm^{-1}, respectively. Unless otherwise stated a $\Delta E = 210$ cm^{-1} and $\eta = 1.18$ is used throughout this paper for all calculations at 300 K.

D. Isotopic enrichments

Calculated results for isotopic enrichments at low pressures for ''scrambled'' systems with large mole fractions of heavy isotopes are given in Table V and Fig. 7. They were obtained from individual isotopomeric rate constants using Eqs. (4.18a), (4.18b), and (4.26) of Ref. 36 for the enrichments.[86] The individually calculated rate constants used for the enrichment calculations are listed in Tables III and IV. Results are also given in Fig. 7 using $\eta = 1$ for comparison with $\eta = 1.18$.

TABLE III. Reaction rate coefficients for ozone formation processes relative to $^{16}O + {}^{32}O_2 \rightarrow {}^{48}O_3$ at low pressure.

Reaction	Expt.[a]	Calc.
$^{16}O + {}^{16}O{}^{16}O$	1.00	1.00
$^{17}O + {}^{17}O{}^{17}O$	1.02	1.02
$^{18}O + {}^{18}O{}^{18}O$	1.03	1.03
$^{18}O + {}^{16}O{}^{16}O$	0.93	0.93
$^{17}O + {}^{16}O{}^{16}O$	1.03	1.03
$^{18}O + {}^{17}O{}^{17}O$	1.03	1.07
$^{17}O + {}^{18}O{}^{18}O$	1.31	1.39
$^{16}O + {}^{17}O{}^{17}O$	1.23	1.38
$^{16}O + {}^{18}O{}^{18}O$	1.53	1.53
$^{16}O + {}^{16}O{}^{17}O$ [b]	1.17	1.19
$^{16}O + {}^{16}O{}^{18}O$ [b]	1.27	1.25
$^{17}O + {}^{16}O{}^{17}O$ [b]	1.11	1.04
$^{17}O + {}^{17}O{}^{18}O$ [b]	1.21	1.20
$^{18}O + {}^{16}O{}^{18}O$ [b]	1.01	0.99
$^{18}O + {}^{17}O{}^{18}O$ [b]	1.09	1.05
$^{16}O + {}^{17}O{}^{18}O$ [b]	—	1.43
$^{17}O + {}^{16}O{}^{18}O$ [b]	—	1.21
$^{18}O + {}^{16}O{}^{17}O$ [b]	—	1.01

[a]From Mauersberger *et al.*, Ref. 26, at room temperature.
[b]This rate constant here is the sum of both channels, $X + YZ \rightarrow XYZ$ and $X + YZ \rightarrow XZY$. Each of the rate constants were calculated separately, with the non-RRKM correction applied to any symmetric channel.

E. Pressure effect on the enrichment $^{18}\delta$ and individual rate constant ratios

The rate constants for reactions $^{16}O + {}^{18}O{}^{18}O \rightarrow {}^{16}O{}^{18}O{}^{18}O$ and $^{18}O + {}^{18}O{}^{18}O \rightarrow {}^{18}O{}^{18}O{}^{18}O$ were calculated

TABLE IV. Reaction rate coefficients for asymmetric and symmetric channels of recombination reactions, relative to $^{16}O + {}^{16}O_2 \rightarrow {}^{16}O_3$ at low pressure.

Reaction	Expt.[a]	Calc.
Symmetric products		
$^{16}O + {}^{17}O{}^{16}O \rightarrow {}^{16}O{}^{17}O{}^{16}O$	—	0.51
$^{16}O + {}^{18}O{}^{16}O \rightarrow {}^{16}O{}^{18}O{}^{16}O$	0.54 ± 0.01	0.52
$^{17}O + {}^{16}O{}^{17}O \rightarrow {}^{17}O{}^{16}O{}^{17}O$	—	0.51
$^{17}O + {}^{18}O{}^{17}O \rightarrow {}^{17}O{}^{18}O{}^{17}O$	—	0.51
$^{18}O + {}^{16}O{}^{18}O \rightarrow {}^{18}O{}^{16}O{}^{18}O$	0.52 ± 0.01	0.52
$^{18}O + {}^{17}O{}^{18}O \rightarrow {}^{18}O{}^{17}O{}^{18}O$	—	0.52
Asymmetric products[b]		
$^{18}O + {}^{17}O{}^{16}O \rightarrow {}^{18}O{}^{17}O{}^{16}O$	—	0.47
$^{18}O + {}^{18}O{}^{16}O \rightarrow {}^{18}O{}^{18}O{}^{16}O$	0.46 ± 0.03	0.47
$^{17}O + {}^{18}O{}^{16}O \rightarrow {}^{17}O{}^{18}O{}^{16}O$	—	0.52
$^{17}O + {}^{17}O{}^{16}O \rightarrow {}^{17}O{}^{17}O{}^{16}O$	—	0.53
$^{18}O + {}^{18}O{}^{17}O \rightarrow {}^{18}O{}^{18}O{}^{17}O$	—	0.53
$^{18}O + {}^{16}O{}^{17}O \rightarrow {}^{18}O{}^{16}O{}^{17}O$	—	0.53
$^{17}O + {}^{16}O{}^{18}O \rightarrow {}^{17}O{}^{16}O{}^{18}O$	—	0.70
$^{16}O + {}^{16}O{}^{17}O \rightarrow {}^{16}O{}^{16}O{}^{17}O$	—	0.68
$^{17}O + {}^{17}O{}^{18}O \rightarrow {}^{17}O{}^{17}O{}^{18}O$	—	0.70
$^{16}O + {}^{18}O{}^{17}O \rightarrow {}^{16}O{}^{18}O{}^{17}O$	—	0.69
$^{16}O + {}^{16}O{}^{18}O \rightarrow {}^{16}O{}^{16}O{}^{18}O$	0.73 ± 0.02	0.74
$^{16}O + {}^{17}O{}^{18}O \rightarrow {}^{16}O{}^{17}O{}^{18}O$	—	0.74

[a]From Janssen *et al.*, Ref. 27. See also Ref. 85 for a definition of the value used for the particular rate constant.
[b]Reactions are ordered in the sequence of an increasing zero-point energy difference.

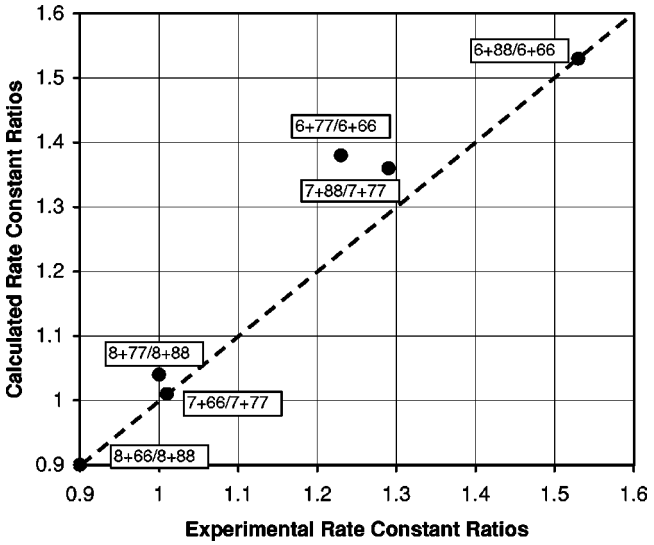

FIG. 5. A comparison of calculated and experimental (Ref. 26) ratios of the recombination rate constants, k_{X+YY}/k_{X+XX}, at 300 K.

as a function of pressure and used to obtain the pressure dependence of the rate constant ratios, $k_{6,88}/k_{6,66}$ and $k_{8,66}/k_{8,88}$. The calculated and experimental results are compared in Fig. 8.

Recombination rate constants for the reactions $^{16}O+{}^{16}O^{18}O\rightarrow{}^{16}O^{16}O^{18}O$, $^{16}O+{}^{16}O^{18}O\rightarrow{}^{16}O^{18}O^{16}O$ and $^{18}O+{}^{16}O^{16}O\rightarrow{}^{16}O^{16}O^{18}O$ were also obtained as a function of the pressure, and used to calculate the pressure dependence of the enrichment of the isotopic combination $^{16}O^{18}O^{16}O+{}^{16}O^{16}O^{18}O$, using Eq. (4.18a) of Ref. 36. The experimental and calculated results are compared in Fig. 9.

F. Temperature effect on isotopic enrichments and on individual rate constant ratios

Both η and ΔE can in principle be temperature dependent, and data on two Y+XX→YXX reactions at a second temperature are needed to determine that dependence. In the current absence of such data, we assume that ΔE is relatively temperature independent in the interval 140–300 K and then fit the experimental enrichment of $^{16}O^{16}O^{18}O$ at 140 K. We obtain an $\eta=1.13$ at 140 K. Predicted rate constant ratios for recombinations at 140 K are given in Table VI, using $\eta=1.13$ and $\Delta E=210$ cm^{-1}.

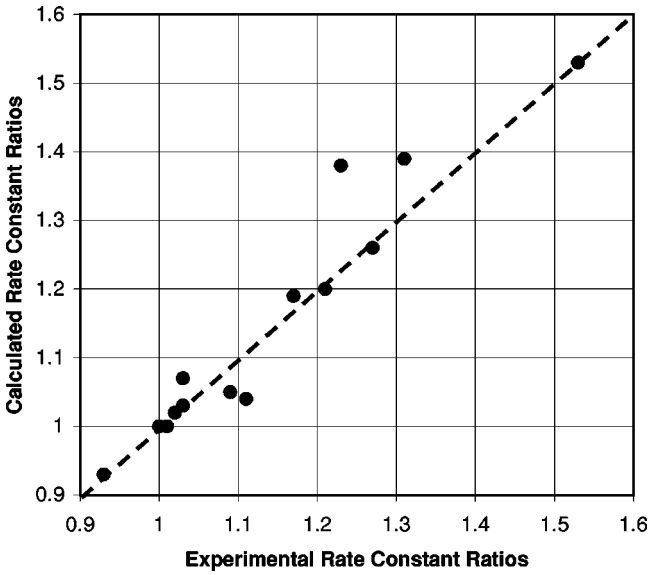

FIG. 6. A comparison of calculated and experimental (Ref. 26) ratios of the recombination rate constants, k_{X+YZ}/k_{6+66}, at 300 K. Some of the experimental rate constants are "derived quantities."[26]

TABLE V. Calculated and experimental isotopic enrichments at 300 K.

Isotope combination	Experiment[a]	Calc.[b] (%)
$^{16}O^{16}O^{16}O$	0.0	0.0
$^{17}O^{17}O^{17}O$	−1.8	−2.1
$^{18}O^{18}O^{18}O$	−4.6	−4.7
$^{16}O^{16}O^{17}O$ [c]	11.3	12.3
$^{16}O^{16}O^{18}O$ [c]	13.0	12.7
$^{17}O^{17}O^{16}O$ [c]	12.1	12.2
$^{17}O^{17}O^{18}O$ [c]	9.5	10.4
$^{18}O^{18}O^{16}O$ [c]	14.4	12.7
$^{18}O^{18}O^{17}O$ [c]	8.3	9.2
$^{16}O^{17}O^{18}O$ [c]	18.1	17.4

[a]Experimental data at 300 K are from Mauersberger *et al.*, Ref. 26.
[b]Calculated from Eqs. (4.18a), (4.18b), and (4.26) of Part I. The definition of enrichment is given by Eq. (4.13) there.
[c]Enrichment is for all possible isotopomers.

G. Recombination rate constant for $^{16}O+{}^{32}O_2\rightarrow{}^{48}O_3$

The rate constant for the recombination reaction $^{16}O+{}^{32}O_2\rightarrow{}^{48}O_3$ is calculated using the hindered-rotor and, for comparison, the free rotor, transition states, together with the weak collision assumption and the step-ladder energy transfer model. The calculated values of k_{bi}^0 given in Table I are compared there with the experimental values and with results obtained from the strong collision model. For comparison with the results for $\Delta E=210$ cm^{-1}, values of ΔE of 180 and 250 cm^{-1} were also used and are given in Table I, footnote *c*. In the case of $^{16}O+{}^{32}O_2\rightarrow{}^{48}O_3$ the results using a free rotor ("loose") transition state are found to be the same as those obtained using a hindered-rotor transition state and the same ΔE: The values of k_{bi}^0 for the free rotor are 5.2×10^{-12} cm^{-6}

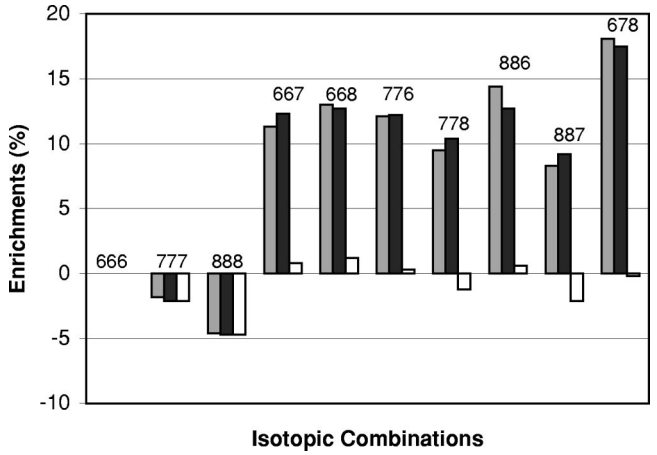

FIG. 7. Experimental[26] (gray bars) and calculated isotopic enrichments for scrambled systems enriched in heavy isotopes at 300 K, with $\eta=1.18$ (dark bars) and $\eta=1$ (light bars), respectively.

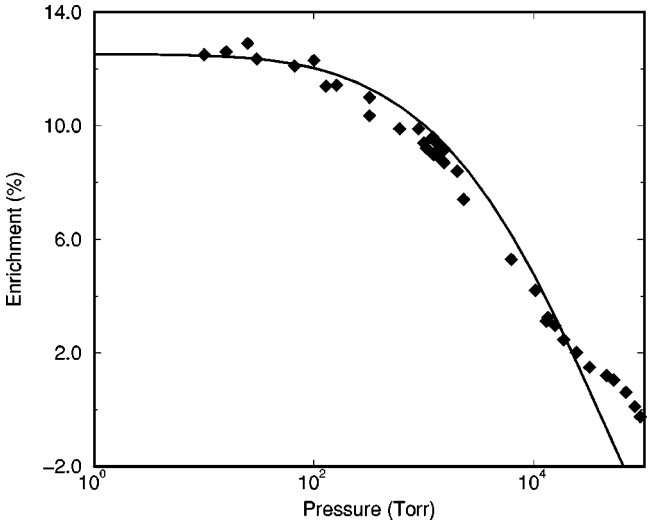

FIG. 8. The pressure dependence of the ratios of recombination rate constants. The filled circles and triangles are the experimental results (Ref. 28) for the rate constant ratios of $^{18}O+^{32}O_2 \rightarrow ^{18}O^{16}O^{16}O$ and $^{18}O+^{36}O_2 \rightarrow ^{54}O_3$, and $^{16}O+^{36}O_2 \rightarrow ^{18}O^{18}O^{16}O$ and $^{16}O+^{32}O_2 \rightarrow ^{48}O_3$, respectively. The solid lines are the calculated results using the hindered-rotor transition state.

s^{-1} at 130 K and 0.76×10^{-12} cm^{-6} s^{-1} at 300 K, using the $\eta=1.13$ obtained at 130 K in Sec. IV F, in exact agreement with the hindered rotor results in Table I.

The pressure dependence of the rate constant for the reaction $^{16}O+^{32}O_2 \rightarrow ^{48}O_3$ was calculated at 130 K and 300 K using the methods described in Sec. II. The experimental and calculated pressure dependence are compared in Fig. 10.

IV. DISCUSSION

A. The effects of symmetry

There is reasonable agreement in Figs. 5–9 for the ratios of the recombination rate constants for the formation of the ozone isotopomers, the enrichments, and for the pressure effects. Two ''symmetry driven'' isotopic effects occur: (1) the difference in zero-point energies of the two exit channels of the asymmetric isotopomers causes the partitioning factors Y_a and Y_b to differ from 1/2, resulting in a large unconventional mass-dependent effect for the rate constant ratios in unscrambled systems. (2) An η-effect ($\eta\cong1.18$ at 300 K) also occurs, reducing the recombination rate for the symmetric isotopomers XYX at low pressures. The possible origin of the η-effect is a larger deviation from RRKM behavior for the symmetric species[1,36,37] or a collisional effect:[1,87,88] In principle, the lower density of states of symmetric molecules could make the collisional energy transfer less efficient for these molecules and thus make ω smaller. Since a collisional frequency, such as ω, and ρ occur as a product in the expressions for the rate constants, one may not be able to distinguish between an effect on ρ and an effect on ω on the basis of current kinetic data alone. Experiments discussed later

TABLE VI. Temperature effect on enrichments and rate constant ratios.

	Cal. (140 K)	Expt. (140K)[a]	Cal. (300 K)	Expt. (300K)[b]
η	1.13[c]	–	1.18[d]	–
$^{16}O+^{16}O^{18}O/^{16}O+^{16}O^{16}O$	0.75	–	0.74	0.73
$^{18}O+^{16}O^{16}O/^{16}O+^{16}O^{16}O$	0.83	–	0.93	0.93
$^{16}O+^{18}O^{16}O/^{16}O+^{16}O^{16}O$	0.52	–	0.52	0.54
Enrichment of $^{16}O^{16}O^{18}O$	8.2%	8.3%	12.7%	13.0%
$^{16}O+^{18}O^{18}O/^{16}O+^{16}O^{16}O$	1.53	–	1.53	1.53
$^{18}O+^{18}O^{16}O/^{16}O+^{16}O^{16}O$	0.44	–	0.47	0.46
$^{18}O+^{16}O^{18}O/^{16}O+^{16}O^{16}O$	0.52	–	0.52	0.52
Enrichment of $^{16}O^{18}O^{18}O$	3.0%	–	14.1%	14.4%
$^{18}O+^{18}O^{18}O/^{16}O+^{16}O^{16}O$	1.03	–	1.03	1.03
Enrichment of $^{18}O^{18}O^{18}O$	−16.6%	–	−4.7%	−4.6%

[a]Experimental results are taken from Ref. 12.
[b]Experimental results are taken from Ref. 26.
[c]Obtained by fitting the experimental value of the isotopic enrichment of $^{16}O^{16}O^{18}O$ at 140 K.
[d]Obtained by fitting the experimental value of two rate constant ratios, $^{16}O+^{18}O^{18}O/^{16}O+^{16}O^{16}O$ and $^{18}O+^{16}O^{16}O/^{18}O+^{18}O^{18}O$, at 300 K.

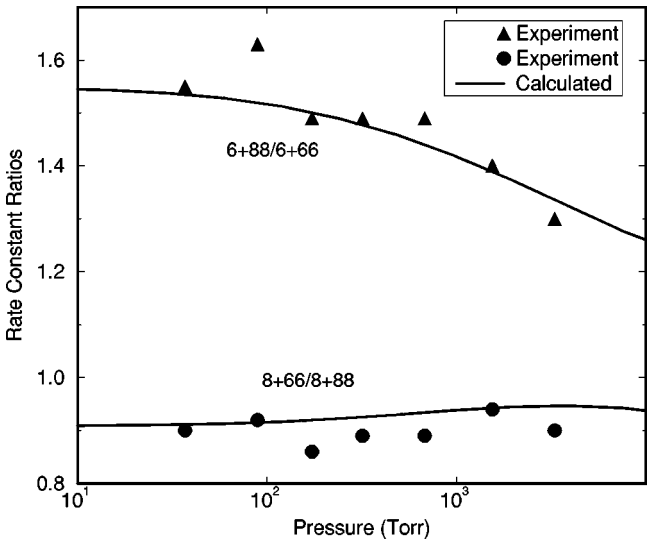

FIG. 9. The pressure dependence of the enrichment $^{18}\delta$. The filled diamonds are the experimental results (Ref. 28) and the solid line gives the calculated results using the hindered-rotor transition state.

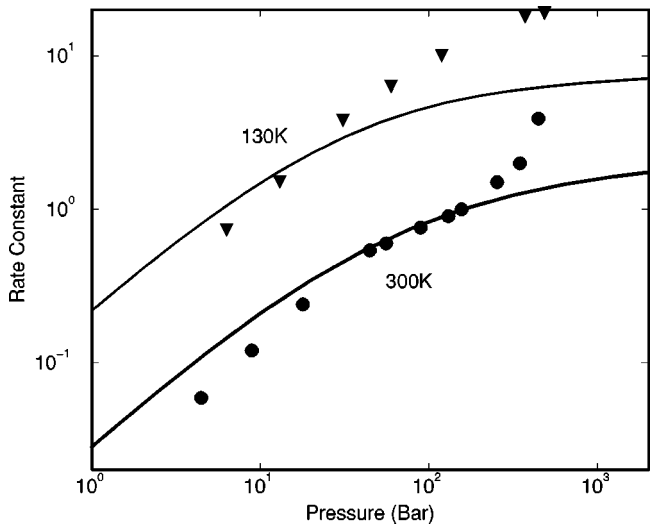

FIG. 10. The pressure dependence of the recombination rate constant for $^{16}O+^{32}O_2 \rightarrow ^{48}O_3$ at 130 K and 300 K. The units are 10^{-12} cm^{-3} $molecule^{-1}$ s^{-1}. The experimental data are taken from Ref. 31.

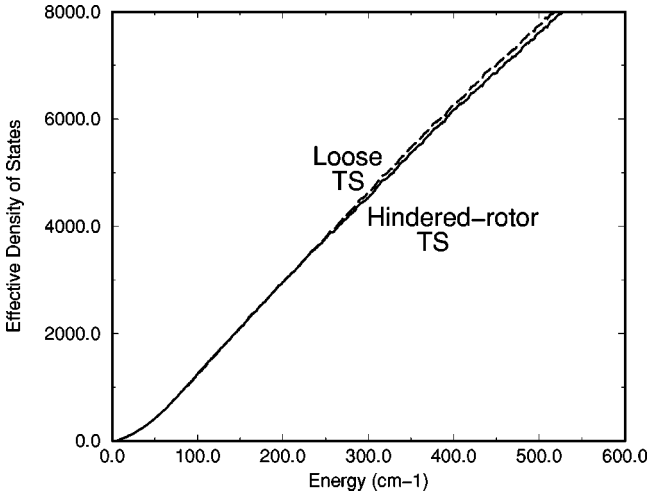

FIG. 11. The effective density of states $\Sigma_J \rho(EJ)h[N(EJ)]$ as a function of R for the recombination reaction $^{16}O+^{32}O_2 \rightarrow ^{48}O_3$, where h is the unit step function. The dashed and solid curves are obtained using free rotor and hindered-rotor transition states, respectively. The E's are given relative to the lowest state of the separated O and O_2.

would distinguish them. In the meanwhile from an operational viewpoint the precise origin of η does not affect the present predictions.

B. Weak collision aspect and temperature effect

The present weak collision assumption provides an explanation of the large negative temperature dependence of the recombination rate constant at low pressures. The experimental rate constant for $^{16}O+^{32}O_2 \rightarrow ^{48}O_3$ at 300 K in Table I is about 8 times slower than that at 130 K, and the weak collision model [Eq. (2.32)] yields a factor of 6 at low pressures. In contrast, when a strong collision assumption is used, the calculated ratio is less than 2. In the present theory the large observed negative temperature coefficient thus arises from the fact that at the higher temperatures more energetic ozone states are populated but only a smaller fraction can be stabilized by a single collision when ΔE is small.

When the weak collision assumption is used it was seen in Table I (footnote c) that the choice of transition state for $^{16}O+^{32}O_2 \rightarrow ^{48}O_3$ has effectively no effect on the low-pressure recombination rate constant and on its temperature dependence: The weak collision permits only ozone states with low energies to be stabilized in a single collision, and at low energy the transition state is largely ''loose.'' Thus, the free rotor transition state theory and the more realistic hindered-rotor theory yield similar results.

The individual rate constants at low pressures are determined approximately by the integral of $(\omega_d - \omega_a)\Sigma_J \rho Y_a e^{-E/k_B T}$ over energy, as in Eq. (2.32). The latter integral depends on the transition state via the partitioning factor Y_a. In the case of a symmetric molecule, the ratio reduces to a heaviside step function $h(N_a)$ multiplied by 1/2, and is then relatively insensitive to the choice of the transition state. This behavior is easily understood using Fig. 11. In this figure the free and hindered-rotor transition states are compared for the effective density of states $\Sigma_J \rho(EJ)h(N_a)$ for the formation of $^{48}O_3$. Due to the weak collision effect they differ very little, especially at energies lower than 300 cm^{-1}. As a result, the calculated recombination rate constant for a symmetric molecule is almost independent of the nature of the transition state at low pressures.

The effect of pressure on an asymmetric reaction is somewhat different: For an asymmetric molecule, the Y_a depends on the functional form of N's. The ratios of rate constants for the two different entrance channels thereby show a somewhat greater dependence on the nature of the transition state. In particular the low-pressure experimental results of the rate constant ratios could be fitted using the free rotor transition state, but using $\Delta E = 260$ cm^{-1} instead of $\Delta E = 210$ cm^{-1} for the hindered-rotor transition state. An explanation for the best fit ΔE being smaller for the hindered-rotor transition state is given in Ref. 89.

Since the negative temperature dependence of the recombination rate constant at low pressures for $^{16}O+^{32}O \rightarrow ^{48}O_3$ in the present model is mainly due to the small value of ΔE,[90] one expects the negative temperature coefficient to be less when this collisional deactivation of ozone does not affect the rate. Indeed, the ΔE is absent in Eq. (2.39) for the isotopic exchange reaction and the experimental ratio of the exchange rate constants at 130 K and 300 K for $^{16}O+^{18}O^{18}O \rightarrow ^{16}O^{18}O+^{18}O$ is about 1.9. It is substantially smaller than the experimental factor of 8 found for the low-pressure recombination. In terms of a T^{-m} behavior of the rate constant, the coefficient m obtained in the present calculations is 0.53 for the isotopic exchange reaction, and 2.2 for the low-pressure recombination reaction, as compared with the experimental values of 0.88 ± 0.26 and 2.6, respectively. In the case of isotopic exchange reaction, the negative temperature dependence in the present theory arises from the increasingly hindered rotation with increasing T, due to the well known tightening effect of the transition state with increasing temperature.[67–79]

The pressure dependence of the ozone recombination reaction was studied experimentally for the reaction $^{16}O+^{32}O_2 \rightarrow ^{48}O_3$ at various temperatures. However, only at temperatures below 160 K was a simple unimolecular reaction dependence on pressure observed. At higher temperatures there is a sudden rise in a log–log plot of the rate–pressure curves at very high pressures, whose source is uncertain.[31] Nevertheless, the data do indicate a less negative temperature dependence at higher pressures than that at low pressures.[31]

C. Ratios of recombination rate constants

The isotopic effect on the ratios of the individual recombination rate constants at 300 K is dramatic. The rate constant for the channel with the lower zero-point energy for the fragments is substantially larger than that for the other channel. The weak collision enters importantly into the explanation, since the calculated differences in the rate constant ratios at 300 K are too small in the strong collision limit.[37] The reason is that the higher energy states are now accessible for recombination in the strong collision limit, and they have $Y_a \approx 1/2$. For example, the calculated ratios of the rate constants for $^{16}O+^{18}O^{18}O \rightarrow ^{16}O^{18}O^{18}O/^{16}O+^{32}O_2 \rightarrow ^{48}O_3$ and $^{18}O+^{18}O^{16}O \rightarrow ^{16}O^{18}O^{18}O/^{16}O+^{32}O_2 \rightarrow ^{48}O_3$ are 1.27 and

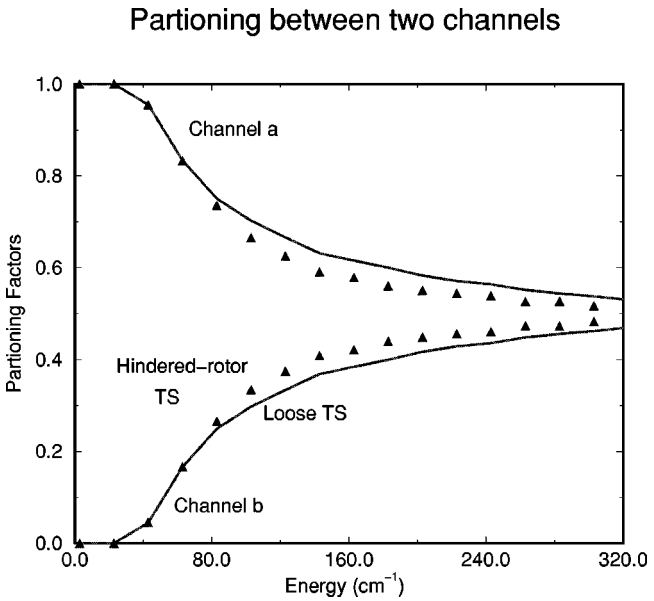

FIG. 12. Density-weighted partitioning factors $\Sigma_J \rho(EJ) Y_{a,b} / \Sigma_J \rho(EJ)$ are plotted vs energy. The zero of the energy at $J=0$ is that for the channel with the smaller zero-point energy. The solid lines and the triangles are obtained using free rotor and hindered-rotor transition states, respectively.

0.58, respectively, when the strong collision is used. These results differ relatively little from 1.18 and 0.59, the ratios expected from an η-effect alone.

Insight into how a small difference in zero-point energy can produce a large difference in a rate constant ratio is provided by Fig. 12. The J-averaged quantity $\Sigma_J \rho e^{-E/k_B T} Y_a / \Sigma_J \rho$ is plotted there as a function of E. For a better understanding of how a small difference between the zero-point energies dramatically influences Y_a and Y_b at the relevant energies plots are given in Fig. 13 using a simple model for N_a and N_b: The N_a (N_b) is assumed to be a quadratic function of $E - E_a(E_b)$ with E_a (E_b) being the threshold energy for dissociation via channel a (b). This approximate quadratic behavior of N_a and N_b above the

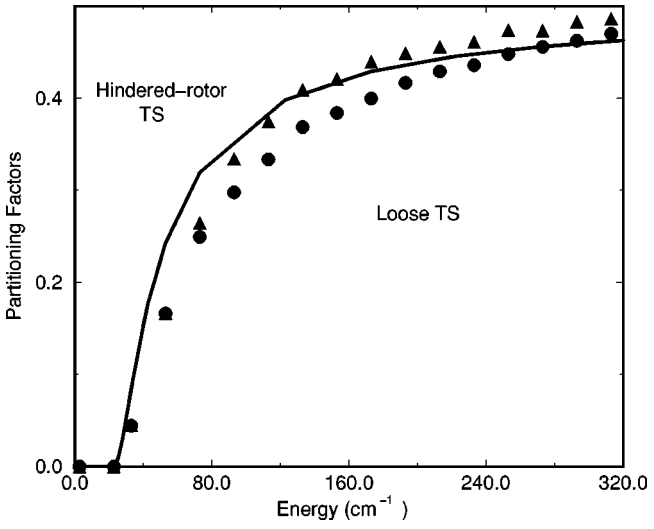

FIG. 13. Density-weighted partitioning factors, $\Sigma_J \rho(EJ) Y_b(EJ) / \Sigma_J \rho(EJ)$, are plotted vs energy. The points are the same as in Fig. 12 for the channel with a larger zero-point energy, channel b.

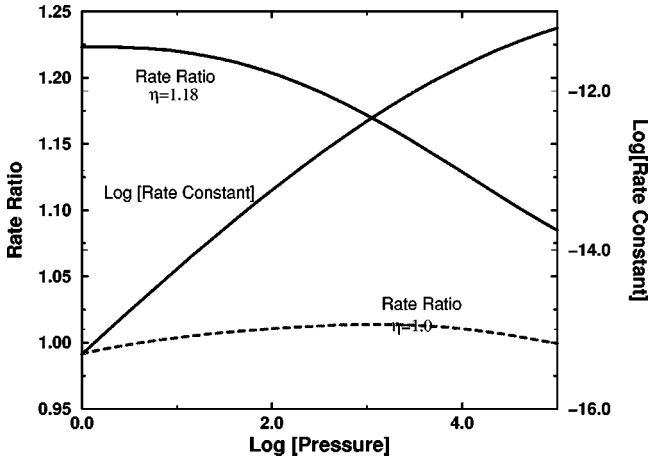

FIG. 14. Results for a model for the pressure effects on the rate constant and the rate constant ratios, $(k^{as}_{6,68} + k^{as}_{8,66})/k_{6,66}$. The high-pressure limit for the recombination rate constant is taken as 2×10^{-11} cm^{-3} s^{-1}. The curves are described in the text.

threshold is readily understood in terms of a crude model.[91] Because of the quadratic behavior a small difference of the zero-point energy causes a relatively large difference between the rate constants for the two channels, even for energies up to 300 cm^{-1}, since it magnifies the effect of the differences in the partitioning factors Y_a and Y_b, as seen in Fig. 13.

D. Pressure effects

Pressure effects were investigated for the ^{18}O enrichment in the $^{16}O^{16}O^{18}O + {}^{16}O^{18}O^{16}O$,[28] the rate constant ratios, $k_{16,1818}/k_{16,1616}$ and $k_{18,1616}/k_{18,1818}$,[28] and the formation rate constant of $^{48}O_3$.[31] The experimental and calculated results are in reasonable agreement (Figs. 8–10). Some discrepancy exists between the calculated and experimental results for the pressure effect on the recombination rate constant for $^{16}O + {}^{32}O \rightarrow {}^{48}O$ in Fig. 10. Its origin is presently speculative.[92]

A striking feature of the pressure effects is that the effect on the rate constant ratio $k_{16,1818}/k_{16,1616}$ and on the enrichment is evident at pressures lower than that on the $^{16}O + {}^{16}O^{16}O$ recombination rate constant: A large effect of pressure on the first two is apparent at 10^2 Torr, but that on $k^{rec}_{6,66}$ becomes evident only at 10^4 Torr (cf. Figs. 8–10). Some insight into this difference in pressure effects is obtained by noting that the rate constant ratios in Fig. 8 and the enrichments in Fig. 9 are each the ratios of two slopes of rate constant versus pressure plots, since both the numerator and denominator in each are proportional to ω at low pressures. Changes in slopes are more easily detected than any deviation from linearity of a log k_{bi} versus log pressure curve, as can also be seen from their comparison in Fig. 14.

The pressure effect seen in Fig. 8 for 8+66/6+66 can be understood as follows: An 866* molecule formed from a b channel 8+66 can dissociate via two exits at any given energy above the dissociation threshold, just as a 666* can. There are two opposing effects of increasing pressure on the ratio: It increases Y_b because of increased mean energy but the increased pressure decreases the η-effect and hence de-

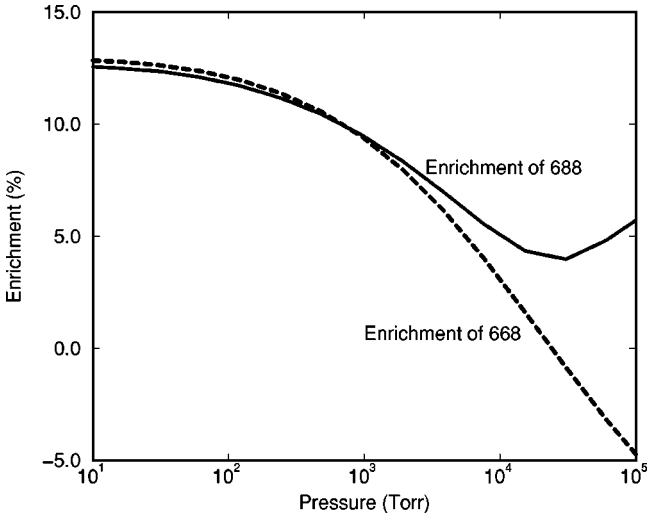

FIG. 15. A comparison between the calculated pressure dependence of the enrichment of $^{50}O_3$, namely $^{16}O^{16}O^{18}O$ and $^{16}O^{18}O^{18}O$ (i.e., $^{16}O^{16}O^{18}O + {}^{16}O^{18}O^{16}O$ and $^{16}O^{18}O^{18}O + {}^{18}O^{16}O^{18}O$).

creases the ratio. The net ratio of rate constants is then almost pressure-independent.[93] In contrast, when a 688* is formed from an a channel 6+88, the 688* can dissociate at low energies only via one exit channel, 6+88, and so its mean lifetime is longer than that of 666*. The ratio of their rate constants is therefore high at low pressures. The pressure effects of a Y_a decreasing to 1/2 (higher energy) and a decreasing η-effect now reinforce each other. Thus, the 6+88/6+66 ratio decreases substantially with increased pressure, as in Fig. 8.

The ratio $k_{bi}^{\mathrm{eff}}/k_{bi}^{\mathrm{sym}}$, given by $\int_0^\infty \omega(N_a+N_b)/[\omega+(N_a+N_b)/\eta\rho]/\int_0^\infty \omega N/[\omega+(N)/\rho]$, where $N=2N_a$, is plotted in Fig. 14 as a function of pressure.[94] The results for $\eta=1$ and $\eta=1.18$ are contrasted there for the rate constant ratios and show, thereby, that the η-effect is essential for interpreting the large pressure dependence of the enrichment. The contribution to the enrichment from the symmetric term such as the $k_{6,q6}^s/k_{6,66}^s$ in Eq. (2.13) of Ref. 36 is approximately pressure-independent and so does not contribute to the pressure effect. The dependence of enrichment on pressure in Fig. 9 is also observed in a strong collision calculation: While a strong collision model is inadequate for treating Y_a or Y_b alone and hence for treating the effect of pressure on the individual rate constant ratios, it is found to be adequate for the enrichment, since the latter involves the Y's only via the sum, Y_a+Y_b, which is unity, and so does not influence the pressure effect. The pressure effect on the enrichment of $^{16}O^{18}O^{18}O+{}^{18}O^{16}O^{18}O$ is also calculated in the present study, and compared in Fig. 15 with the pressure dependence of the enrichment of $^{16}O^{16}O^{18}O+{}^{16}O^{18}O^{16}O$.

E. The potential energy surface, η, and ΔE

Most of the important experimental results in the present study are obtained at the low-pressure limit, and so are fortunately relatively insensitive to the type of transition state and thus to the details of the potential energy surface. Further, the transition state is almost loose for low energy states, which are the only important states in the weak collision case. In contrast, the temperature dependence of the isotopic exchange reaction rate constant is sensitive to the potential energy surface. It does not suffer the complicated behavior of the high-pressure recombination rate constant, and so was used to provide an "effective" potential energy surface. The latter was in turn used in the calculation of the recombination reaction rate constants. Repeating the calculations when an improved potential energy surface is published would be of interest.

Most of the experimental data treated in the present study are obtained at 300 K and the η and ΔE for this temperature were chosen to fit the two rate constant ratios, $^{16}O+{}^{18}O^{18}O/{}^{16}O+{}^{16}O^{16}O$ and $^{18}O+{}^{16}O^{16}O/{}^{18}O+{}^{18}O^{18}O$. They were then applied to obtain all other reaction rate constants, and from them, the isotopic enrichments. It would be desirable to have similar data on these two rate constant ratios at other temperatures, which would provide information on the temperature dependence of η and ΔE in the present model. Currently, experimental results in the temperature range of 140 to 373 K, have been reported for the temperature dependence of the enrichment of $^{16}O^{16}O^{18}O$.[12] We obtained an η of 1.13 at 140 K by fitting the experimental enrichment $^{18}\delta$, assuming $\Delta E=210$ cm^{-1}. It yields the predictions in Table VI.

The 210 cm^{-1} for ΔE and other values in the range 180 to 250 cm^{-1} gave reasonable agreement with experiment for the rate constant for the low-pressure recombination reaction of $^{16}O+{}^{32}O_2\rightarrow{}^{48}O_3$ at both 130 K and 300 K and gave the correct negative temperature dependence of the latter. These values of ΔE are also not inconsistent with classical trajectory energy transfer studies for highly excited ozone molecules: In classical trajectory studies on the collisional energy transfer between highly energetic ozone molecules and Ar, He, and N_2, it was found that an averaged magnitude of the energy transferred per collision (but both deactivation and activation collisions are counted) is about 0.4 k_BT at 2500 K ($\sim$600 cm^{-1}) and 0.5–0.6 k_BT at 500 K ($\sim$200 cm^{-1}).[95]

It would be particularly helpful to obtain ΔE and η independently. For example, in a pump–dump laser experiment or a direct overtone experiment a vibrationally-excited ozone molecule could be produced in the ground electronic state with an energy just above the threshold. The real-time behavior of the dissociating ozone could be studied to see if it were bi- or multi-exponential rather than single exponential. Again if an asymmetric isotopomer such as $^{16}O^{16}O^{18}O$ were studied similarly, measurement of the ratio of the yields of $^{16}O^{16}O$ and $^{16}O^{18}O$ in real time would provide a direct measure of the partitioning effect and its energy dependence. Direct studies of ΔE would be helpful, but of the small amounts of ΔE rather than of the rare "supercollisions" studied in the vibrational energy transfer to CO_2.[96]

From a theoretical viewpoint classical trajectories can reveal the biexponentiality, as reported recently by Schinke and co-workers.[66] For the η-factor, however, suitably rotationally averaged and state-averaged quantum mechanical results may be needed. In this case one should treat not only states produced in scattering calculations but also states of

ozone which might be nondissociative even they satisfy the (EJ) requirement for dissociation.

If the η-effect reflected a long-lived region of the phase space of ozone, or in quantum mechanical terms long-lived resonances, then at sufficiently low pressures they too would contribute to recombination and cause η to approach unity. Only if some long-lived states were completely decoupled dynamically from the dissociation products would η differ from unity at very low pressures. However, studies at low pressure can be complicated by increased participation of wall reactions.

In contrast, if the η-effect is due to collisions then no approach of η to unity would be expected at very reduced pressures. Of course, at sufficiently low pressures a stabilization would occur by a radiative rather than by a collision.

We have formulated the present theory so as to be more general than for ozone formation. A mass-independent enrichment may occur via a transfer of ozone effect to other molecules, such as possibly in CO_2, via $O_3+h\nu\rightarrow O_2+O(^1D)$ followed by $O(^1D)+CO_2\rightarrow O(^3P)+CO_2$. It may also occur directly via reactions such as $O+SiO\rightarrow OSiO^*$ or $O+XO_n\rightarrow XO_{n+1}^*$, where X is another element, and the product XO_n^* is symmetric. The latter may be stable or unstable species. Similar remarks apply to sulphides, such as $S+XS\rightarrow SXS^*$, and the stabilized SXS could also undergo a further chemical reaction. The field of recombination of isotopically symmetric or a symmetric intermediates has the promise of providing a very rich one for further experimental and theoretical investigation, with implications for atmospheres as well as for meteorites.[2]

ACKNOWLEDGMENTS

It is a pleasure to acknowledge the support of this research by the National Science Foundation. The present work owes much to[36,37] Dr. Bryan Hathorn.

APPENDIX A: THE EIGENVALUES OF A HINDERED ROTOR

For the orbital-hindered rotational part of the Hamiltonian, we use body-fixed axes with the line of centers **R** between the atom and the diatomic molecule serving as the body-fixed z-axis. Apart from the kinetic energy for the radial coordinate R, the Hamiltonian H can be written as

$$H=\left(\frac{\mathbf{j}^2}{2I}+\frac{\mathbf{l}^2}{2\mu R^2}\right)\hbar^2+V(r,R,\theta), \tag{A1}$$

where $\mathbf{j}^2$ is the operator for the square of the angular momentum for the diatomic molecule, I moment of inertia of the latter, $\mathbf{l}^2$ the operator of the square of the orbital angular momentum, R the distance between the atom and the center of mass of the diatomic fragment, r the instaneous bond length of that fragment, and θ the angle between **R** and **r**, the vector along the axis of the diatomic molecule. We transform from a space-fixed $|jlm_jm_l\rangle$ representation to another space-fixed $|jlJM_j\rangle$ representation,[97–100] and then from the latter to a body-fixed representation $|jJM_j\Omega\rangle$, where Ω is the component of **J** along the body-fixed z-axis. Since **l** is perpendicular to the body-fixed z-axis, the Ω is also the component of **j** along this z-axis. In this representation $\mathbf{j}^2$ and $\mathbf{J}^2$ are diagonal, but not $\mathbf{l}^2$. In terms of **J** and **j** we have

$$\mathbf{l}^2=(\mathbf{J}-\mathbf{j})\cdot(\mathbf{J}-\mathbf{j})=\mathbf{J}^2-2\mathbf{j}\cdot\mathbf{J}+\mathbf{j}^2. \tag{A2}$$

In body-fixed components $\mathbf{j}\cdot\mathbf{J}$ is $j_zJ_z+j_xJ_x+j_yJ_y$. It equals $j_zJ_z+j_+J_-+j_-J_+$, where $J_\pm=J_x\pm iJ_y$, and similarly for $j_\pm$. They are the usual raising and lowering operators. In the matrix $\langle j'\Omega'|H|j\Omega\rangle$ in the body-fixed $|j\Omega\rangle$ representation the JM_J is suppressed for notational brevity. There is a well known result for the elements diagonal in $\Omega(\Omega'=\Omega)$,[97–100]

$$H_{j\Omega,j'\Omega}=\langle j\Omega|H|j'\Omega\rangle = \left[\frac{j(j+1)}{2I}+\frac{J(J+1)+j(j+1)-2\Omega^2}{2\mu R^2}\right] \times\hbar^2\delta_{jj'}+V_{j\Omega,j'\Omega}. \tag{A3}$$

For the elements off-diagonal in Ω $(\Omega'\neq\Omega)$ we have[97–100]

$$H_{j\Omega,j'\Omega'}=\langle j\Omega|H|j'\Omega'\rangle = -\frac{\hbar^2}{2\mu R^2}[J(J+1)-\Omega\Omega']^{1/2} \times[j(j+1)-\Omega\Omega']^{1/2}\delta_{jj'}\delta_{\Omega'\Omega\pm1}. \tag{A4}$$

The potential energy matrix elements in the body-fixed frame $V_{j\Omega,j'\Omega}$ are given by

$$V_{j\Omega,j'\Omega}=\int\int Y_{j\Omega}^*V(r,R,\theta)Y_{j'\Omega}d(\cos\theta)d\phi, \tag{A5}$$

where the Y's are spherical harmonics. Integration is immediately made over ϕ. For any given Ω the conditions on the matrix elements are that

$$j\geqslant|\Omega|,\ J\geqslant|\Omega|, \tag{A6}$$

and similarly when these quantities have primes.

In calculating the energy levels of the transition state, we neglect the elements off-diagonal in Ω $(\Omega'\neq\Omega)$, and so diagonalize the matrix by setting $|H_{j\Omega,j'\Omega}-E\delta_{jj'}|=0$. The neglect of off-diagonal elements $(\Omega'\neq\Omega)$ in treating the radial motion of the two reactants has been termed in the collision dynamics literature the "j_z-conserving," "coupled state," or "centrifugal decoupling" approximation.[100] Typically a zeroth-order body-fixed description is better at short separation distances R than the space-fixed, and vice versa at large R.[98] At very large initial R, Ω is the projection of **j** and of **J** along the initial wave vector **k**, the initial line of the centers. The evolution of Ω as R decreases is of much interest in a full collision dynamics calculation, but for our statistical calculation we are principally interested in the accessibility of the quantum states rather than in the detailed coupling between states of different Ω's.

When YZ in X+YZ is heteronuclear, the two channels in any state n of the hindered rotor transition state are $X+YZ\rightarrow X\cdots YZ\rightarrow XYZ$ or XZY. They should each be weighted by the square of the hindered-rotor wavefunction, integrated over the solid angle leading to the respective product 2π for each product. Ultimately we plan to make such a calculation, but for the present paper we adopted a simpler

though more approximate approach which does not involve these integrated wavefunctions, as in the use of the weighting factor of 1/2 in Eqs. (2.14) and (3.2).

In the present formulation we have used R as the reaction coordinate. It is known that when the transition state becomes sufficiently tight the distance between the atoms becomes a better approximation to the reaction coordinate because it provides a deeper minimum of $N(q)$ at $q=q^{\dagger}$.[77–79] The Hamiltonian then becomes more complicated, however. Thus, even with an accurate potential energy surface the use of R as a reaction coordinate would not necessarily give an accurate value of N_{EJ} in the transition state.

APPENDIX B: DERIVATION OF EQ. (2.11)

From Eq. (2.15) we have

$$\omega(E'J'\rightarrow EJ)=\omega_d t(J'\rightarrow J)\,\delta(E'-E-\Delta E) \tag{B1}$$

and

$$\omega(EJ\rightarrow E'J')=\omega_a t(J\rightarrow J')\,\delta(E-E'+\Delta E). \tag{B2}$$

Because of microscopic reversibility we have

$$\sum_{J'J}\omega(E'J'\rightarrow EJ)\rho(E'J')e^{-E'/k_BT}$$

$$=\sum_{J'J}\omega(EJ\rightarrow E'J')\rho(EJ)e^{-E/k_BT}. \tag{B3}$$

When the strong collision is introduced for the transfer of rotational energy one obtains

$$\sum_{J'J}\omega_d\delta(E'-E-\Delta E)\rho(E'J')e^{-E'/k_BT}(2J+1)$$

$$\times e^{-E_J/k_BT}=\sum_{J'J}\omega_a\delta(E-E'+\Delta E)\rho(EJ)$$

$$\times e^{-E/k_BT}(2J'+1)e^{-E'_J/k_BT}, \tag{B4}$$

i.e.,

$$\omega_d\delta(E'-E-\Delta E)\sum_{J'}\rho(E+\Delta E,J')e^{-(E+\Delta E)/k_BT}$$

$$=\omega_a\delta(E-E'+\Delta E)\sum_{J}\rho(EJ)e^{-E/k_BT}, \tag{B5}$$

and so

$$\omega_d\sum_{J'}e^{-\Delta E/k_BT}\rho(E+\Delta E,J')=\omega_a\sum_{J}\rho(EJ). \tag{B6}$$

This result yields Eq. (2.16) of the text.

APPENDIX C: DERIVATION OF THE LOW-PRESSURE RECOMBINATION RATE CONSTANT

The states above the dissociation threshold are divided into open and closed states, and their steady-state equations are given by Eqs. (2.23) and (2.31), respectively. The states below the dissociation threshold contain only closed states, with population densities described by Eqs. (2.27)–(2.28). We combine these equations for an M-ladder system with $N-1$ of them below the dissociation threshold.

To derive Eq. (2.32) and higher approximations, we first consider the region $E_n<D_0$. From Eq. (2.27) we have

$$\omega_d g_{n+1}-\omega g_n+\omega_a g_{n-1}=0. \tag{C1}$$

The flux S is given by Eq. (2.29) and is also given by

$$S=\omega_d g_{n+1}-\omega_a g_n=\omega_d g_1 \quad (1\leqslant n\leqslant N-1). \tag{C2}$$

When multiplied by $(\omega_d/\omega_a)^n$ the first half of Eq. (C2) can be rewritten as

$$(\omega_d/\omega_a)^n S=\omega_a[(\omega_d/\omega_a)^{n+1}g_{n+1}-(\omega_d/\omega_a)^n g_n]. \tag{C3}$$

Upon summing over n from 1 to p, where $p\leqslant N-1$, we obtain

$$S=\frac{(\omega_d-\omega_a)g_{p+1}}{1-(\omega_a/\omega_d)^p}=\omega_d g_1 \quad (1<p\leqslant N-1). \tag{C4}$$

To make contact with the formalism in a recent paper[60] we note that Eq. (C4) can be rewritten in terms of a diffusion coefficient $k_{\rm diff}^N$ defined in (3.16) there. In the present notation it is

$$k_{\rm diff}^N=\omega_d/\sum_{n=1}^{N}(\omega_a/\omega_d)^{n-1}$$

$$\equiv(\omega_d-\omega_a)/[1-(\omega_a/\omega_d)^N]. \tag{C5}$$

Thus, the flux S in Eq. (C4) can be written as the $k_{\rm diff}^N g_N$, as also in Eq. (3.15) of Ref. 60.

We next consider the derivation of Eq. (2.32). For that purpose we truncate the Eqs. (2.23) by setting $g_{N+2}=0$. This system of Eqs. (2.23) then reads as

$$-\omega g_{N+1}+P_{N+1}^c\omega_a g_N=-\omega g_{N+1}^o, \tag{C6}$$

$$P_N^c\omega_d g_{N+1}-\omega g_N+P_N^c\omega_a g_{N-1}=-\omega g_N^o. \tag{C7}$$

The population density g_{N+1} can be eliminated from the two equations, yielding

$$(\omega-P_N^cP_{N+1}^c\omega_a\omega_d/\omega)g_N-P_N^c\omega_d g_{N-1}$$

$$=P_N^c\omega_d g_{N+1}^o+\omega g_N^o. \tag{C8}$$

When Eqs. (C4) for $p=N-1$ and $N-2$ are introduced into Eq. (C8), and when we write $g_N\cong g_{N-1}=S/(\omega_d-\omega_a)$, Eq. (C8) yields, to an adequate approximation,

$$S=\frac{\omega g_N^o+P_N^c\omega_d g_{N+1}^o(\omega_d-\omega_a)}{\omega_a+P_N^o\omega_d-P_N^cP_{N-1}^c\omega_a\omega_d/\omega}. \tag{C9}$$

Typically, the product of the P^c's in the denominator can be neglected (cf. Fig. 16), yielding Eq. (2.32) upon integration over E.

APPENDIX D: SOLUTION OF THE RECOMBINATION RATE CONSTANT AT AN ARBITRARY PRESSURE

The solution for g_1 can be written as the ratio between the determinants of the matrices **B** and **A**, where the elements of **A** are $A(i,i)=1$ $(i=1,2,...,M)$, $A(i,i-1)=-V_i(i=2,3\ldots,M)$, $A(i+1,i)=-W_i(i=1,2,\ldots,M-1)$,

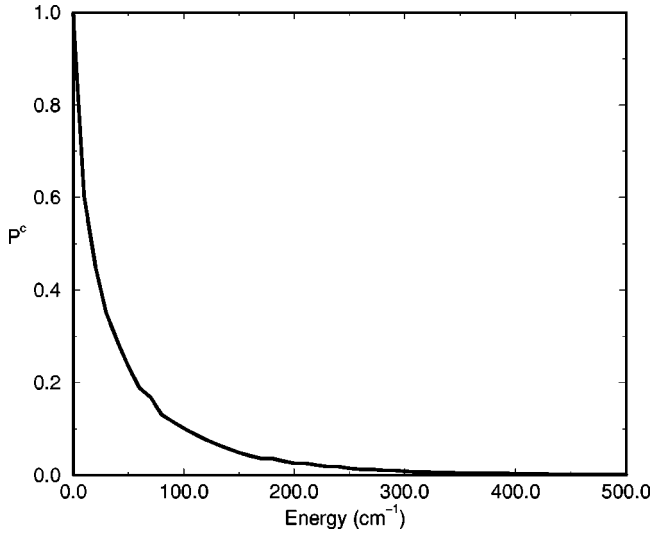

FIG. 16. P^c is plotted as a function of energy.

and all other elements vanish, the V_i and W_i being defined in Eqs. (2.21)–(2.22). Thus, **A** is a tridiagonal band matrix. The elements of **B** are the same as those of **A**, except for those in the first column, which are $B(i,1)=U_i$, the U_i being given by Eq. (2.20). The elements of both **A** and **B** are functions of energy. The **B** and **A** thus differ from the **B** and **A** defined in Appendix B.

The rate constant can then be obtained as an integral over all energies in the range of 0 to ΔE:

$$k_{bi}=\int_0^{\Delta E}\omega_d|\mathbf{B}|/|\mathbf{A}|dE. \tag{D1}$$

The $|\mathbf{B}|/|\mathbf{A}|$ in Eq. (D1) contains a sum of terms E_{M+n}, $n=1,2,3,\ldots$.

APPENDIX E: THE POTENTIAL ENERGY SURFACE

A model potential[101] $V(R,r,\theta)=V_{bf}(R)+V_{\text{bend}}(R;\theta)$ is used, where R is the center to center distance between the oxygen atom and the fragment oxygen molecule. The R serves as the reaction coordinate, θ is the angle between the line along the axis of the diatomic molecule and the line of the centers of mass of the two collision particles, $V_{\text{bf}}(R)$ is a bond–fission potential, and $V_{\text{bend}}(R,\theta)$ is a bending potential. The dependence of $V(R,r,\theta)$ on the variation in bond length r of each given fragment oxygen molecule is neglected. The $V_{\text{bf}}(R)$ is chosen to be $-C_6/R^6$ for large R, using the $C_6=27.6$ eV Å^6 obtained from the collision cross-section for $O+O_2$.[102] For small R's, $V_{\text{bf}}(R)$ is chosen to be a Morse potential function,[103] $V_{\text{bf}}(R)=D[1-\exp(-\beta(R-R_e)]^2$,[101] where the dissociation energy $D=9107$ cm^{-1},[53] $\beta=2.88$ Å^{-1},[104] and the equilibrium value of R, $R_e=1.667$ Å.[53] The two V_{bf}'s are matched at $R=2.6$ Å. The bending potential is chosen to be[105]

$$V_{\text{bend}}(R;\theta)=V_R(1-\cos^4\theta),$$
$$V_R=V_0\exp[-\alpha(R-R_0)]. \tag{E1}$$

The parameters are chosen to be the isotopic exchange reaction rate constant at 300 K and its temperature dependence are roughly consistent with the experimental values. When R_0 is taken as 2.6 Å, V_0 has a value of 0.35 eV, and α is 5.5 Å^{-1}. For a comparison, some calculations are in progress using the potential energy surface given in Ref. 65.

[1] Y. Q. Gao and R. A. Marcus, Science **293**, 259 (2001).
[2] R. N. Clayton, L. Grossman, and T. K. Mayeda, Science **182**, 485 (1973).
[3] J. E. Heidenreich, III and M. H. Thiemens, J. Chem. Phys. **78**, 892 (1983).
[4] J. E. Heidenreich, III and M. H. Thiemens, J. Chem. Phys. **84**, 2129 (1986).
[5] K. Mauersberger, Geophys. Res. Lett. **14**, 80 (1987).
[6] J. Yang and S. Epstein, Geochim. Cosmochim. Acta **51**, 2011 (1987).
[7] J. Yang and S. Epstein, Geochim. Cosmochim. Acta **51**, 2019 (1987).
[8] M. H. Thiemens and T. Jackson, Geophys. Res. Lett. **14**, 624 (1987).
[9] M. H. Thiemens and T. Jackson, Geophys. Res. Lett. **15**, 639 (1988).
[10] S. M. Anderson, J. Morton, and K. Mauersberger, Chem. Phys. Lett. **156**, 175 (1989).
[11] J. Morton, B. Schueler, and K. Mauersberger, Chem. Phys. Lett. **154**, 143 (1989).
[12] J. Morton, J. Barnes, B. Schueler, and K. Mauersberger, J. Geophys. Res. **95**, 901 (1990).
[13] M. H. Thiemens and T. Jackson, Geophys. Res. Lett. **17**, 717 (1990).
[14] B. Schueler, J. Morton, and K. Mauersberger, Geophys. Res. Lett. **17**, 1295 (1990).
[15] J. Wen and M. H. Thiemens, Chem. Phys. Lett. **172**, 416 (1990).
[16] J. Wen and M. H. Thiemens, J. Geophys. Res. **96**, 10911 (1991).
[17] S. M. Anderson, K. Mauersberger, J. Morton, and B. Schueler, ACS Symp. Ser. **502**, 155 (1992).
[18] M. H. Thiemens, ACS Symp. Ser. **502**, 138 (1992).
[19] K. Mauersberger, J. Morton, B. Schueler, and J. Stehr, Geophys. Res. Lett. **20**, 1031 (1993).
[20] D. Krankowsky, F. Bartecki, G. G. Klees, K. Mauersberger, and K. Schellenbach, Geophys. Res. Lett. **22**, 1713 (1995).
[21] J. Sehested, O. J. Nielsen, H. Egsgaard, N. W. Larsen, T. Pedersen, L. K. Christensen, and M. Wiegell, J. Geophys. Res. **100**, 20979 (1995).
[22] D. Krankowsky and K. Mauersberger, Science **274**, 1324 (1996).
[23] L. K. Christensen, N. W. Larsen, F. M. Nicolaisen, T. Pedersen, G. O. Sørensen, and H. Egsgaard, J. Mol. Spectrosc. **175**, 220 (1996).
[24] J. C. Johnson and M. H. Thiemens, J. Geophys. Res. **102**, 25395 (1997).
[25] S. M. Anderson, D. Hüsebusch, and K. Mauersberger, J. Chem. Phys. **107**, 5385 (1997).
[26] K. Mauersberger, B. Erbacher, D. Krankowsky, J. Günther, and R. Nickel, Science **283**, 370 (1999).
[27] C. Janssen, J. Günther, D. Krankowsky, and K. Mauersberger, J. Chem. Phys. **111**, 7179 (1999).
[28] J. Guenther, B. Erbacher, D. Krankowsky, and K. Mauersberger, Chem. Phys. Lett. **306**, 209 (1999).
[29] J. Günther, D. Krankowsky, and K. Mauersberger, Chem. Phys. Lett. **324**, 31 (2000).
[30] M. R. Wiegell, N. W. Larsen, T. Pedersen, and H. Egsgaard, Int. J. Chem. Kinet. **29**, 745 (1997).
[31] M. Hippler, R. Rahn, and J. Troe, J. Chem. Phys. **93**, 6560 (1990).
[32] M. H. Thiemens, Science **283**, 341 (1999) and references cited therein.
[33] J. Farquhar, H. M. Bao, and M. H. Thiemens, Science **289**, 756 (2000).
[34] H. Bao, M. H. Thiemens, J. Farquhar, D. A. Campbell, C. C.-W. Lee, K. Heine, and D. B. Loope, Nature (London) **406**, 176 (2000).
[35] M. H. Thiemens, T. Jackson, E. C. Zipf, P. W. Erdman, and C. van Egmond, Science **270**, 969 (1995).
[36] B. C. Hathorn and R. A. Marcus, J. Chem. Phys. **111**, 4087 (1999).
[37] B. C. Hathorn and R. A. Marcus, J. Chem. Phys. **113**, 9497 (2000).
[38] J. Troe, J. Chem. Phys. **66**, 4745 (1977).
[39] J. Troe, J. Chem. Phys. **66**, 4758 (1977).
[40] J. Troe, J. Chem. Phys. **77**, 3485 (1982).
[41] J. Troe, J. Chem. Phys. **85**, 1708 (1986).
[42] W. Schranz and S. Nordholm, Int. J. Chem. Kinet. **13**, 1051 (1981).
[43] I. Oref, J. Chem. Phys. **77**, 5146 (1982).
[44] R. G. Gilbert and S. C. Smith, *Theory of Unimolecular and Recombination Reactions* (Blackwell Scientific Publications, Boston, 1990), and references cited therein.
[45] P. J. Robinson and K. A. Holbrook, *Unimolecular Reactions* (Wiley-Interscience, London, 1972) and references cited therein.
[46] D. C. Tardy and B. S. Rabinovitch, J. Chem. Phys. **48**, 1282 (1968).
[47] D. C. Tardy and B. S. Rabinovitch, J. Chem. Phys. **45**, 3720 (1966).

[48] I. Oref and D. C. Tardy, Chem. Rev. **90**, 1282 (1990).
[49] T. Baer and W. L. Hase, *Unimolecular Reaction Dynamics, Theory and Experiment* (Oxford University Press, New York, 1996), and references cited therein.
[50] R. A. Marcus, J. Chem. Phys. **20**, 359 (1952).
[51] R. A. Marcus, J. Chem. Phys. **43**, 2658 (1965); **52**, 1108 (1970).
[52] S. C. Smith and R. G. Gilbert, Int. J. Chem. Kinet. **20**, 979 (1988).
[53] J. I. Steinfeld, S. M. Alder-Golden, and J. W. Gallagher, J. Phys. Chem. Ref. Data **16**, 911 (1987), and references cited therein.
[54] S. M. Anderson, F. S. Klein, and F. Kaufman, J. Chem. Phys. **83**, 1648 (1985).
[55] From the definition of $g(EJ)$, we have a differentiation, $dg(EJ)/dt = -c(EJ)/([X][YZ])^2 d([X][YZ])/dt + dc(EJ)/dt/[X][YZ]$. The second term on the right hand side gives rise to the right hand side of Eq. (2.6), while the first term can be rewritten as $-c(EJ)/[X][YZ]k_{bi}$. This first term is typically small, relative to each of the terms on the right hand side of Eq. (2.6), and can be neglected. In fact, in the typical experiments (Ref. 19) for the measurement of the ozone formation rate constant, the term can be shown to be less than one thousandth of the other terms.
[56] For example, R. A. Marcus, J. Chem. Phys. **43**, 2658 (1965), Eq. (A2), where a degeneracy $\Omega(E^\dagger)$ appears instead of a step function. However, in the present equation (2.9) each degenerate state adds a unity to the sum. When there is nuclear tunneling through the effective barrier, the sum is replaced by a series of tunneling factors, κ, as in Eq. (3) of R. A. Marcus, J. Chem. Phys. **45**, 2138 (1966). In the classical limit for the q-motion, the κ's become the step functions of Eq. (2.9).
[57] If the body-fixed component K of the total angular momentum J, involving the rotation of the energetic ozone molecule about the axis with the smallest moment of inertia, were also assumed to be constant during the lifetime of the hot ozone molecule, each $N(EJ)$ would be replaced by $N(EJK)$ and the summation in Eq. (2.39) would be over J and K. In the unimolecular dissociation/bimolecular recombination literature K is usually treated as "active" (not as a constant), and we do also.
[58] M. Quack and J. Troe, Ber. Bunsenges. Phys. Chem. **78**, 240 (1974).
[59] When YZ is heteronuclear some of the quantum states in the hindered rotor X···YZ arise not only from XZY*→X···YZ but also from the distinguishable dissociation, XZY*→X···ZY. A more accurate value of word than 1/2 would be obtained using the weighting function (cf. Appendix A).
[60] R. A. Marcus and Y. Q. Gao, J. Chem. Phys. **114**, 9807 (2001).
[61] All states with $E_n < D_0$ are closed. D_0 is the dissociation energy at $J=0$ of the ozone isotopomer to form the diatomic molecule with the smaller zero-point energy.
[62] When two of the three isotopes are present in trace amounts, the enrichment is calculated from Eqs. (4.18a) and (4.18b) for E_{ijj}, and (4.26) for E_{ijk} for unequal i, j, and k in Ref. 37. In Eqs. (4.18a) and (4.18b), $k^{\rm as}_{\rm X,YZ}$ is the rate constant for X+YZ→XYZ, while in Eq. (4.26) each $k^{\rm as}$ denotes the total formation rate constant for the sum of the two isotopomeric ozone molecules, in this case XYZ and XZY. The enrichment E_{ijj} is readily shown later in Ref. 86 to be the same as ${}^i\delta$ when $j=16$ and when i (=17 or 18) is only present in trace amounts. The derivation of Eqs. (4.18) and (4.26) in Ref. 36 involved treating a large number of permutations of isotopes in the ozone, in the oxygen molecule, and in the atom, and was simplified by an approximation, good to a few parts per thousand, that related each isotopic oxygen atom concentration to isotopic oxygen molecule concentrations.
[63] K. Yamashita, K. Morokuma, F. Le Quere, and C. Leforestier, Chem. Phys. Lett. **191**, 515 (1992); C. Leforestier, F. Le Quere, K. Yamashita, and K. Morokuma, J. Chem. Phys. **101**, 3806 (1994).
[64] Y. Q. Gao, W. Chen, and R. A. Marcus (unpublished). The modified *ab initio* potential (Ref. 65) yielded the k_{ex} for 6+88→8+68 as follows: 1.94×10^{-12} cm^{-3} s^{-1} at 300 K and 2.61×10^{-12} cm^{-3} s^{-1} at 130 K. The temperature coefficient is 0.35.
[65] A. Gross and G. D. Billing, Chem. Phys. **217**, 1 (1997).
[66] R. Siebert, R. Schinke, and M. Bitterova, Phys. Chem. Chem. Phys. **4**, 1795 (2001).
[67] W. L. Hase, J. Chem. Phys. **64**, 2442 (1976).
[68] M. Quack and J. Troe, Ber. Bunsenges. Phys. Chem. **81**, 329 (1977).
[69] G. P. Smith and D. M. Golden, Int. J. Chem. Kinet. **10**, 489 (1978).
[70] S. N. Rai and D. G. Truhlar, Int. J. Chem. Kinet. **79**, 6046 (1983).
[71] S. W. Benson, Can. J. Chem. **61**, 881 (1983).
[72] W. L. Hase and D. M. Wardlaw, in *Bimolecular Collisions*, edited by J. E. Baggott and M. N. Ashfold (Royal Society of Chemistry, Burlington House, London, 1989), p. 171.
[73] X. Hu and W. L. Hase, J. Phys. Chem. **93**, 6029 (1989).
[74] D. M. Wardlaw and R. A. Marcus, Adv. Chem. Phys. **70**, 231 (1988).
[75] S. J. Klippenstein and R. A. Marcus, J. Chem. Phys. **91**, 2280 (1989).
[76] S. J. Klippenstein and R. A. Marcus, J. Chem. Phys. **93**, 2418 (1990).
[77] S. J. Klippenstein, J. Chem. Phys. **94**, 6469 (1991).
[78] S. J. Klippenstein and Y.-W. Kim, J. Chem. Phys. **99**, 5790 (1993).
[79] S. J. Klippenstein, in *The Chemical Dynamics and Kinetics of Small Radicals, Part I*, edited by K. Liu and A. Wagner (World Scientific, Singapore, 1995), and references cited therein.
[80] W. Forst, *Theory of Unimolecular Reactions* (Academic, New York, 1973) and references cited therein.
[81] B. C. Hathorn and R. A. Marcus, J. Phys. Chem. A **105**, 2612 (2001).
[82] C. Califano, *Vibrational States* (Wiley, London, 1976), p. 215.
[83] V. G. Tyuterev, S. Tashkun, P. Jensen, A. Barbe, and T. Cours, J. Mol. Spectrosc. **198**, 57 (1999).
[84] The fitting parameters $hc\omega_i$'s and hcx_{ij}'s are given in the following in units of cm^{-1}: $hc\omega_1=716.6$, $hc\omega_2=1136.1$, $hc\omega_3=1071.4$, $hcx_{11}=-1.477$, $hcx_{22}=-4.497$, $hcx_{33}=-7.358$, $hcx_{12}=-8.087$, $hcx_{13}=-16.66$, $hcx_{23}=-37.87$.
[85] These rate constants differ slightly from those in Ref. 25, where an extra factor of 2 was added in the definition of the rate constant. In the present case, we have defined the rate constant so as not to include the factor of 2, in conformity with Ref. 26.
[86] We note in passing that the enrichment E defined by Eq. (4.13) of Ref. 36 reduces to the enrichment δ defined by Eq. (2.12) in that reference when ^{17}O and ^{18}O are present in trace amounts: The $({}^M{\rm O}_3)_{\rm meas}$ in the former equals for trace isotope Q, OQO+QOO, and further $({}^M{\rm O}_3/{}^{48}{\rm O}_3)_{\rm cal} = (3/2){\rm QO}/{\rm O}_2$, since statistically, i.e., neglecting any isotopic effect, the equilibrium constant $({\rm QO}_2)_{\rm tot}({\rm O}_2)/({\rm O}_3)({\rm OQ}) = ({\rm QOO}+{\rm OQO})({\rm O}_2)/({\rm O}_3)({\rm OQ}) = 1+1/2 = 3/2$, on introducing the symmetry factors. Thereby, Eq. (4.13) of Ref. 36 yields $E = ({}^M{\rm O}_3/{}^{48}{\rm O}_3)_{\rm meas}/(3{\rm QO}/2{\rm O}_2) - 1 = 2({\rm QO})({\rm OQO}+{\rm QOO})/3({\rm O}_3)({\rm O}_2) - 1 = \delta$.
[87] The vibrational states are, labeled from 1 to 35, (010), (100), (020), (110), (002), (030), (200), (120), (012), (040), (210), (102), (130), (300), (022), (050), (220), (112), (140), (310), (004), (032), (202), (060), (230), (400), (122), (150), (014), (320), (042), (212), (070), (240), (104).
[88] G. I. Gellene, Science **274**, 1344 (1996) and references cited therein.
[89] Both N_a and N_b for the hindered rotor transition state (TS) increase more slowly with energy than they do for the free rotor TS, since the hindrance of the rotation permits fewer states (cf. Fig. 2). Correspondingly, the difference between N_a and N_b for the hindered-rotor is shown in the following to decrease more rapidly as a function of energy than that for the free rotor and so a smaller ΔE is needed. For example, if N_a and N_b are both written as a function of its excess energy above the threshold: $N_a = (E - E_0^a)^n$ and $N_b = (E - E_0^b)^n$, then at energy E where $E - E_0^a = \epsilon$, $E - E_0^b$ equals $\epsilon - \epsilon_0$, where $\epsilon_0 = E_0^b - E_0^a$. The ratio between the number of states for the two channels becomes $(1 - \epsilon_0/\epsilon)^n$. For a fixed value of this quantity, when n is smaller, ϵ is smaller, and n for the hindered-rotor is smaller than that for the free one. A comparison for the values of N_a calculated using the free and hindered-rotor transition states is very similar to that depicted in Fig. 3.
[90] When a strong collision assumption is used, the present expression reduces to that in Refs. 36 and 37, $k_{bi}^{0,a} = \omega/2\Sigma_J \int_0^\infty \rho e^{-E/k_{\rm B}T}\, dE/Q_a$.
[91] We consider the free rotor transition state to illustrate this approximately quadratic behavior: The number of rotational states of the diatomic molecule with energy less than or equal to ϵ is $\int_0^\epsilon (2j+1)(dj/dE)dE$, where $E = j(j+1)\hbar^2/2I$. This result equals $(2I/\hbar^2)\epsilon$, and the excess energy ϵ equals $E - E_c - E_0$, where E_c is the sum of the centrifugal potential and the loose transition state attractive potential for this channel, $l(l+1)\hbar^2/2\mu R^2 - C_6/R^6$. This R is determined variationally by finding the maximum of this potential barrier. The E_c is then found to vary as l^3. If now we weight this number of states by $\rho(EJ)$, where ρ is approximately a constant times $2J+1$, and let $J \approx l$ since $l \gg j$, then we have an integral over $(2l+1)dl$. When the earlier l^3 term is approximately replaced by an l^2 term with the same maximum magnitude and the integral evaluated, it is found that $N_{a(b)}$ is a quadratic function of $E - E_0^{a,b}$.
[92] If an additional non-RRKM effect, which reduces the effective density of states for both symmetric and asymmetric species, were included, the k_{bi} is decreased at low pressures and less affected at high pressures. Because

of extensive cancellation, the calculated low-pressure results for individual rate constant ratios are unaffected. Further, the same effect would result if η were attributed to less effectiveness in deactivating collisions of the symmetric ozone, since ω and ρ occur as a product.

[93] At higher pressures, the contribution to the recombination reaction from higher energy states with Y_b closer to 1/2, tends to increase the rate constant ratio 8+66/6+66. However, an increased pressure also decreases the effect of η on the recombination rate constants and so tends to reduce the value of the ratio 8+66/6+66. In the high-pressure limit, the effect of η disappears entirely because the ρ term in the expression for the rate constant becomes negligible compared to the collisional term.

[94] In Eq. (2.13) of Ref. 36, this ratio of k_{bi}^{sym} is $2k_{6,q6}^{s}/k_{6,66}^{s}$, and the ratio of $k_{bi}^{\mathrm{eff}}/k_{bi}^{\mathrm{sym}}$ is the $(k_{6,q6}^{\mathrm{as}}+k_{q,66}^{s}K_{\mathrm{ex}})/k_{6,66}^{s}$ there.

[95] A. J. Stace and J. N. Murrell, J. Chem. Phys. **68**, 3028 (1978).

[96] For example, C. A. Michaels, A. S. Mullin, J. Park, J. Z. Chou, and G. W. Flynn, J. Chem. Phys. **108**, 2744 (1998), and references therein.

[97] R. W. Anderson, V. Aquilanti, S. Cavalli, and G. Grossi, J. Phys. Chem. **97**, 2443 (1993).

[98] R. E. Wyatt, J. Chem. Phys. **56**, 390 (1972).

[99] G. C. Schatz and A. Kuppermann, J. Chem. Phys. **65**, 4642 (1976).

[100] R. B. Walker and J. C. Light, Chem. Phys. **7**, 84 (1975).

[101] D. M. Wardlaw and R. A. Marcus, J. Chem. Phys. **83**, 3462 (1985).

[102] B. Brunetti, G. Liuti, E. Luzzatti, F. Pirani, and F. Vecchiocattvi, J. Chem. Phys. **74**, 6734 (1981).

[103] For $R \geqslant 2.6$ Å, the $V_{\mathrm{bf}}(R)$ is written as $-[(1-a)V_1+aV_2]$, where V_1 is the C_6/R^6 term and V_2 is the Morse potential, and a is a function of R, $a=\exp[-6(R-2.6)]$.

[104] The β is obtained from $\beta=[f_{rr}/2D_{OO-O}]^{1/2}$, where f_{rr} is the diagonal quadratic stretching force constant and is 6.1164 mdyn $\mathrm{Å}^{-1}$ (Ref. 53) for ozone. The number of significant figures is less than this number would indicate.

[105] A function of $1-\cos^2\theta$ type has frequently been used (Ref. 101). In order to have a larger hindrance, to obtain a temperature dependence in reasonable agreement with the experimental results, a $1-\cos^4\theta$ function was used in this study. The effect of the hindered-rotor potential is seen in Fig. 3.